Title

Restricted Hartree Fock using complex-valued orbitals: a long-known but neglected tool in electronic structure theory.

Journal

The Journal of chemical physics, 142(2)

ISSN

0021-9606

Authors

Small, David W
Sundstrom, Eric J
Head-Gordon, Martin

Publication Date

2015

DOI

10.1063/1.4905120

Peer reviewed

Restricted Hartree Fock using complex-valued orbitals: a long-known but neglected tool in electronic structure theory

David W. Small and Eric J. Sundstrom and Martin Head-Gordon

Department of Chemistry, University of California,

Berkeley, California 94720 and Chemical Sciences Division,

Lawrence Berkeley National Laboratory, Berkeley, California 94720

(Dated: December 16, 2014)

Abstract

Restricted Hartree Fock using complex-valued orbitals (cRHF) is studied. We introduce an orbital pairing theorem, with which we obtain a concise connection between cRHF and real-valued RHF, and use it to uncover the close relationship between cRHF, unrestricted Hartree Fock, and Generalized Valence Bond Perfect Pairing. This enables an intuition for cRHF, contrasting with the generally unintuitive nature of complex orbitals. We also describe an efficient computer implementation of cRHF and its corresponding stability analysis. By applying cRHF to the Be + H_2 insertion reaction, a Woodward-Hoffmann violating reaction, and a symmetry-driven conical intersection, we demonstrate in genuine molecular systems that cRHF is capable of removing certain potential energy surface singularities that plague real-valued RHF and related methods. This complements earlier work that showed this capability in a model system. We also describe how cRHF is the preferred RHF method for certain radicaloid systems like singlet oxygen and antiaromatic molecules. For singlet O_2, we show that standard methods fail even at the equilibrium geometry. An implication of this work is that, regardless of their individual efficacies, cRHF solutions to the HF equations are fairly commonplace.

I. INTRODUCTION

For decades, the Hartree-Fock (HF) method has served electronic structure theory well, and continues to enjoy significant usage today. The HF energy is typically 0.9 to 0.99 times the exact energy, by which it is bounded below. In many instances, widely used procedures, such as the simpler variants of perturbation and Coupled Cluster theories, may be used to economically obtain most of the remaining energy. In many other cases, all of the standard methods, except certain ones that are extremely computationally expensive, are insufficient. These systems are "strongly correlated (SC)," and very often HF itself is blamed for these failures.

It is all but invariable that, in the SC setting, HF orbitals will break spin symmetry if they are allowed to do so. This gives rise to energy lowering in the form of unrestricted HF (UHF) or generalized HF solutions. For SC systems, standard electron-correlation methods tend to fail badly when used in conjuction with restricted orbitals. Hence, the perhaps most prevalent approach here is to let the symmetry breaking (SB) occur and proceed as usual with the standard methods, including Density Functional Theory (DFT). This incurs, among other "contaminations", mixings of exact states of different total spin. Even if the admixed states are low lying, this can be a significant problem if studying the ground state is an important objective.

There have been several efforts towards scalable models that can treat SC systems without incurring spin SB.[1–32] Some of these are rooted in a sort of back-to-basics approach wherein the possibility of creating effective single-reference, restricted-orbital approximations for SC systems is contemplated.[33–64] The idea has met with some early successes, including some favorable results on familiar SC systems once thought to be confined to the unrestricted-orbital domain. It therefore makes sense to study restricted orbitals, particularly those of (real-orbital) restricted HF (RHF), in a wider SC scope.

Optimism here must be cautious due to some fundamental issues with RHF. Some of these relate to the fairly common occurence of artifactual (spatial) SB in RHF calculations. We are working on some aspects of this, to be described in a forthcoming paper,[65] and there we will provide some references for the existing significant body of work on RHF SB. In the present work, we will examine how some of the general RHF problems can be improved by using complex-valued restricted orbitals.

One of the most accessible examples of cRHF's usefulness is the oxygen molecule, which was the inspiration for the present paper. Here, the primary RHF problem is a SB one. Qualitatively, O_2's low-lying states are characterized by the configuration

$$u_c = (1\sigma_g^+)^2(1\sigma_u^+)^2(2\sigma_g^+)^2(2\sigma_u^+)^2(3\sigma_g^+)^2(1\pi_u)^4 \tag{1}$$

along with two electrons occupying two π^* antibonding orbitals, which span a Π_g irreducible representation of the $D_{\infty h}$ point group. This gives rise to four low-lying states: one triplet, $^3\Sigma_g^-$, and three singlets, a doubly degenerate $^1\Delta_g$ and a $^1\Sigma_g^+$. The triplet is the overall ground state and the $^1\Delta_g$ state is the singlet ground state. Being degenerate, there is not a unique wave function to represent this state. However, near its 1.2 Å equilibrium bondlength, two orthogonal wave functions may be selected that are respectively dominated by the following two configurations:

$$\begin{aligned} \Psi_{\Delta_1} &\sim u_c(\pi_x^*\pi_x^* - \pi_y^*\pi_y^*) \\ \Psi_{\Delta_2} &\sim u_c(\pi_x^*\pi_y^* + \pi_y^*\pi_x^*). \end{aligned} \tag{2}$$

In this region, the $^1\Sigma_g^+$ state is dominated by

$$\Psi_\Sigma \sim u_c(\pi_x^*\pi_x^* + \pi_y^*\pi_y^*). \tag{3}$$

In these equations, we use a "$\sim$" because we have simplified the terms by omitting antisymmetrization, normalization, and the spin components.

For the rest of this paper, we use "RHF" and "cRHF" to denote restricted HF with real and complex orbitals, respectively. In the (real) restricted open-shell HF (ROHF) treatment of the triplet, each π^* orbital is singly occupied, and the wavefunction has the proper Σ_g^- symmetry. But in the singlet case, RHF will doubly occupy one orbital, leaving the remaining one unoccupied. If the latter orbital were the one being occupied, a separate, but essentially equivalent RHF solution would result. We have

$$\begin{aligned} \Psi_{\mathrm{RHF1}} &\sim \Psi_{\Delta_1} + \Psi_\Sigma \\ \Psi_{\mathrm{RHF2}} &\sim -\Psi_{\Delta_1} + \Psi_\Sigma. \end{aligned} \tag{4}$$

This details the SB of the RHF wavefunctions.

Conversely, Ψ_{Δ_1} is a linear combination of the two RHF wavefunctions. Thus, a proper approximation for the $^1\Delta_g$ state using real orbitals takes us into the multireference (MR)

realm. Alternatively, consider a substitution of the π_x^* and π_y^* orbitals with

$$\pi_1^* = \pi_x^* + i\pi_y^* \tag{5}$$

and

$$\pi_{-1}^* = \pi_x^* - i\pi_y^*, \tag{6}$$

where $i = \sqrt{-1}$ and normalization has been ignored for simplicity. Another way of understanding these orbitals is that they are antibonding π orbitals formed from the p_1 and p_{-1} atomic orbitals, i.e. the p orbitals with eigenvalues 1 and -1, respectively, for the z-component angular momentum operator $\mathbf{L}_z$. For diatomic molecules, $\mathbf{L}_z$ commutes with the Hamiltonian operator, so we are simply employing symmetry adapted orbitals. This substitution does not alter the orthogonality status of the overall set of orbitals. We can use these orbitals to define a cRHF determinant: $\Psi_{\text{cRHF}} \sim u_c \pi_1^* \pi_1^*$. Noting that $\pi_1^* \pi_1^* = (\pi_x^* \pi_x^* - \pi_y^* \pi_y^*) + i(\pi_x^* \pi_y^* + \pi_y^* \pi_x^*)$, we get

$$\Psi_{\text{cRHF}} \sim \Psi_{\Delta_1} + i\Psi_{\Delta_2}. \tag{7}$$

We see that cRHF can recover the proper symmetry of the singlet ground state, and it has turned a MR problem into a single reference one.

We emphasize that cRHF is not generally able to cure symmetry issues. For example, it cannot achieve the symmetry of the $^1\Sigma_g^+$ state of O_2. In fact, the increased variational freedom of cRHF may increase the possibilities for SB. Nevertheless, it is only natural at this point to contemplate the nature and utility of cRHF in general.

This is not the first time it has been considered. Several early papers explored complex orbitals in various ways.[66–74] Later, cRHF began to be more explicitly investigated.[75–82] cRHF forms one of Fukutome's 8 classes of HF wave functions, where it is called "CCW."[83] In other work, the concept of projected HF was applied to cRHF, wherein the imaginary part of the cRHF wavefunction is discarded and the orbitals are optimized.[84–88] As with other projected HF schemes, this technique captures a significant amount of correlation energy for small systems, but comes with a loss of size consistency. The technique is also included in Projected Quasiparticle Theory.[9,10] cRHF solutions have been found for several systems, including the cyclopropyl cation,[89], ethylene torsion,[90] ethylenedione (OCCO),[91] B_2H_2 and BCH,[92] $SiLi_2$,[93] SiBF,[94] and small hydrogenic systems,[95] while evidence for semi-empirical cRHF solutions was given for several organometallic complexes.[96–98]

Despite this earlier research, cRHF has not found mainstream application. In this paper, we examine cRHF from a modern perspective, and consider several molecular examples that are intended to extend and complement the existing cRHF work. Our aim is to demonstrate that cRHF is a useful member of the set of standard electronic structure theory methods.

II. THEORY

The above O_2 example involves degenerate RHF solutions, and this latter problem is, in fact, quite commonly encountered in the general case, often without any underlying spatial symmetries. It is of particular concern when, upon traversing a reaction coordinate, there are artifactual singularities in the RHF energy, i.e. the lowest RHF energy over a reaction coordinate involves two or more distinct RHF solutions.

Many years ago, Pople considered this phenomenon in an idealized model with two real solutions crossing one another.[75] He found that, in certain cases, the use of complex orbitals would allow the energy to smoothen near the crossing point, somewhat similar to the result one would expect if the real solutions were used in a two-state Configuration-Interaction calculation. This is one of the key demonstrations of the utility of complex restricted orbitals, and merits further investigation along several lines; we will begin by studying cRHF's connection to RHF.

Clearly, complex orbitals are linear combinations of real valued ones. Without further description, such expansions may be rather long and general and, as such, would offer little insight. However, using the invariance of a determinant wave function with respect to choice of basis for the occupied space, it turns out that we may obtain a set of occupied orbitals that may be written very succinctly in terms of real orbitals.

A. Complex-orbitals Pairing Theorem

Complex orbitals are also of interest in UHF and GHF, and we would like our development to be applicable to these theories, too. For this purpose, and because the implications of complex orbitals in UHF and GHF are a little more complicated than in cRHF, it makes sense to keep our discussion quite general for now. To establish an approach for this, consider the following practical situation. Suppose we make a unitary transformation of a set of RHF

orbitals among themselves, such that at least some of the resulting orbitals are complex valued somewhere on their domain. Due to orbital invariance, the determinant formed from the complex-valued orbitals is still essentially an RHF one. A complex-orbital calculation may well produce such a set of orbitals, but the conceptual reduction to RHF would not be evident if we only inspect the orbitals individually. We see that for any complex-orbital calculation, it is important to determine whether or not its results are fundamentally distinct from what we can obtain in a real-orbital calculation. If the answer is "yes", we will refer to the results as being "fundamentally complex". To test for this, we must look at the occupied space as a whole.

We proceed by assuming a given generic occupied space $\mathcal{W}$, even simply thinking of $\mathcal{W}$ as a generic subspace of a complex inner-product space $\mathcal{V}$, which in the orbital context, would be the finite-basis one-electron space. This way, we can subsume cRHF, where we can effectively ignore the spin aspects, and cUHF and cGHF, where spin must not be neglected, into one discussion.

An essential part of the overall fundamental-complexity determination is asking if $\mathcal{W}$ is fundamentally complex. As the above statements suggest, this latter attribute should be defined as $\mathcal{W}$ not having a real basis. Technically, "real" here means invariant with respect to complex conjugation. The latter is quite naturally defined for spatial orbitals, so this idea poses no problems in cRHF; there, fundamental complexity in $\mathcal{W}$ is all we need to consider.

However, the spin parts make things a little more complicated in GHF: just as there is freedom in defining the spin functions/vectors, so it is with complex conjugation there. In this case, the evaluation of $\mathcal{W}$'s fundamental complexity will depend on the choice of complex conjugation. Without going into much detail, one viable approach to the overall fundamental-complexity determination in GHF is to ask if there exists some spin rotation that transforms the occupied space into one having a real basis relative to a fixed complex conjugation. An equivalent, and perhaps more clear, concept is asking if $\mathcal{W}$ has a real basis relative to *some* choice of complex conjugation.

As a matter of completeness, we should give some practical details about complex conjugation. Complex conjugation amounts to an operator acting on the pertinent vector space. In the context of determining fundamental complexity, it is sufficient to identify complex conjugations as the antiunitary, involutory operators. For the general $\mathcal{W}$ picture, we will assume some such choice and label it $\hat{\mathsf{c}}$. In the spin-orbital context, this operator has the

form $\hat{\mathsf{c}}_1 \otimes \hat{\mathsf{c}}_2$, where $\hat{\mathsf{c}}_1$ is the aforementioned "natural" complex conjugation in the spatial part and $\hat{\mathsf{c}}_2$ is some complex conjugation acting on the spin part.

There are various ways of determining if $\mathcal{W}$ has a real basis. One is by establishing P_B, the matrix representation of $\mathcal{W}$'s orthogonal projection operator with respect to any real basis B of $\mathcal{V}$. $\mathcal{W}$ having a real basis is equivalent to P_B being a real matrix. In the orbital context, we can let B be the atomic orbital basis (in the non-cRHF case, this consists of atomic spin orbitals whose associated orthonormal one-electron spin functions α, β are chosen to be invariants of the given $\hat{\mathsf{c}}_2$). Then $P_B = CC^*S$, where C is the occupied-orbital coefficient matrix, $*$ denotes the conjugate transpose, and S is the spin-orbital AO overlap matrix, which is simply the Kronecker product of the 2-by-2 identity matrix and the spatial AO overlap matrix. S is real and full rank (provided any effective linear dependence has been removed in the usual way), so reality of P_B is the same as reality of CC^*. In summary, the constituents of a complex-orbital calculation are fundamentally complex (with respect to the choice of spin-space complex conjugation) if and only if the AO density matrix is complex. We reiterate that this is sufficient in the cRHF case, and note that it is evident in Fukutome's work (under the "CCW" classification).[83]

To move towards a pairing theorem, suppose we have an orthonormal basis $\{\phi_i\}$ for $\mathcal{W}$. Antiunitary operators preserve orthonormality, so $\{\hat{\mathsf{c}}(\phi_i)\}$ is also orthonormal. Each ϕ_i is a linear combination of its real and imaginary parts, which themselves are linear combinations of ϕ_i and $\hat{\mathsf{c}}(\phi_i)$. While this link to real vectors is technically concise, it is insufficient in that the real vectors are not necessarily orthonormal. But, this latter attribute can be obtained if we transform $\{\phi_i\}$ to a different orthonormal basis. Roughly, the idea here is to "diagonalize" $\hat{\mathsf{c}}$ within $\mathcal{W}$, i.e. look for an orthonormal basis $\{\chi_i\}$ such that $\langle\chi_j|\hat{\mathsf{c}}|\chi_i\rangle$ is a diagonal matrix. Then the real and imaginary parts of each χ_i will form a set of strongly orthogonal pairs.

The new basis is written relative to the old as

$$\chi_i = \sum_j U_{ji}\phi_j, \tag{8}$$

where U is a unitary matrix. Using the antilinearity of $\hat{\mathsf{c}}$, we observe that

$$\langle\chi_j|\hat{\mathsf{c}}|\chi_i\rangle = (U^* M \overline{U})_{ji}, \tag{9}$$

where an overline indicates (ordinary) complex conjugation and

$$M_{ji} = \langle\phi_j|\hat{\mathsf{c}}|\phi_i\rangle. \tag{10}$$

In other words, under this change of basis, the starting matrix M is transformed to $U^* M \overline{U}$. Note that $\overline{U}$ is also unitary and M is complex symmetric (but not necessarily Hermitian).

Suppose U is chosen such that $U^* M M^* U$ is diagonal. Taking the transpose, we have that $\overline{U}^* M^* M \overline{U}$ is also diagonal. These two observations suggest that U and $\overline{U}$ might constitute the left and right transformations of a Singular Value Decomposition (SVD) of M, which would be compatible with the way M transforms, thus giving the desired diagonalization. This is indeed the case: the Autonne-Takagi factorization,[99] a particular SVD specialized to the complex-symmetric case, states that there exists a (complex) unitary U such that

$$U^* M \overline{U} = m, \tag{11}$$

where m is real nonnegative diagonal. We note that any SVD computation would give the same m, but considering that the SVD is unique only up to (matching) unitary transformations within the left and right subspaces corresponding to the same singular value, a conventional SVD may not produce the desired U-$\overline{U}$ relationship between its left and right unitary matrices, even if there are no degeneracies among the singular values.

If j is such that $m_{jj} = 1$, then χ_j is real. Otherwise (i.e. $m_{jj} < 1$), χ_j and $\hat{\mathsf{c}}(\chi_j)$ form a linearly independent set. Let

$$\begin{aligned} \mathrm{Re}(\chi_j) &= \frac{1}{2}\left(\chi_j + \hat{\mathsf{c}}(\chi_j)\right) \\ \mathrm{Im}(\chi_j) &= \frac{i}{2}\left(\hat{\mathsf{c}}(\chi_j) - \chi_j\right), \end{aligned} \tag{12}$$

i.e. these are the real and imaginary parts, respectively, of χ_j. We can multiply χ_j by a phase factor such that $\mathrm{Re}(\chi_j)$ and $\mathrm{Im}(\chi_j)$ are orthogonal. We then define

$$\begin{aligned} \eta_j &= N_j \mathrm{Re}(\chi_j) \\ \eta_{\hat{j}} &= N_{\hat{j}} \mathrm{Im}(\chi_j), \end{aligned} \tag{13}$$

where $\hat{j}$ is some unique integer greater than n_o, the dimension of the occupied space, i.e. if $j \neq k$ then $\hat{j} \neq \hat{k}$, and N_j and $N_{\hat{j}}$ are real normalization scalars. $\{\eta_j, \eta_{\hat{j}}\}$ is an orthonormal set of real vectors, and, because χ_j is normalized, we may write

$$\chi_j = \cos(\theta_j)\eta_j - i \sin(\theta_j)\eta_{\hat{j}}, \tag{14}$$

where θ_j is a rotation angle.

Because $\mathrm{span}(\{\eta_j, \eta_{\hat{j}}\}) = \mathrm{span}(\{\chi_j, \hat{\mathsf{c}}(\chi_j)\})$, the full set of η orbitals, including the ones with hatted indices, is orthonormal. We may summarize the above findings as follows:

Any set of occupied complex orbitals can be transformed into a set of complex orbitals, each of which is a linear combination of one or two real orbitals, the real orbitals forming an orthonormal set, with each one being uniquely associated with one of the complex orbitals.

In summary, this result provides an occupied-space basis that is concisely related to a (more familiar and facile) orthonormal real basis.

B. the MR element of cRHF

We now specialize to the cRHF case. Here, it suffices to focus on the spatial parts of the orbitals, so we will now assume that these are denoted by the χ_j. For each doubly occupied pair, the corresponding spatial part of the wave function is

$$\chi_j \chi_j = \Pi_j + \Omega_j, \tag{15}$$

where

$$\Pi_j = \cos^2(\theta_j)\eta_j\eta_j - \sin^2(\theta_j)\eta_{\hat{j}}\eta_{\hat{j}} \tag{16}$$

and

$$\Omega_j = -i\sin(\theta_j)\cos(\theta_j)(\eta_j\eta_{\hat{j}} + \eta_{\hat{j}}\eta_j). \tag{17}$$

The cRHF wavefunction is then simply the (antisymmetrized) product over all pairs of the terms on the RHS of eq. (15) (with an $\alpha\beta$ spin part included for each pair).

Let us compare these cRHF components to the constituents of the Generalized Valence Bond Perfect Pairing (PP)[100] wavefunction. The normalized PP wavefunction is a product of two-electron wave functions, whose spatial parts are written

$$\Pi_j^{(\mathrm{PP})} = \cos(\theta_j)\eta_j\eta_j - \sin(\theta_j)\eta_{\hat{j}}\eta_{\hat{j}}, \tag{18}$$

where we are using the same labeling for the variables to aid in the comparison. In other words, PP is also parameterized by rotation angles and two restricted orbitals per pair. As our notation suggests, the Π_j constituents in cRHF and PP have the same basic form. This helps us understand the driving force for complexification in RHF. The PP wave function incorporates an important piece of the static correlation, and thereby always produces an energy lower than that of RHF. In short, in PP, the θ_j will always be non-zero.

Things are more complicated in cRHF: complexification entails energetically beneficial PP-like terms but also the Ω_j parts, which are of the open-shell-singlet flavor and typically higher in energy. Hence, cRHF, unlike PP, will not always polarize, i.e. RHF is often stable to complexification. For O_2, essentially only one pair complexifies, because therein the PP and open-shell terms are degenerate. In Pople's idealized example, complexification was limited to one pair, whose two associated real orbitals had different spatial symmetries, and this brought the energy of the open-shell part sufficiently low to admit a complex solution.

In the multiple pair case, we may expand out the cRHF product, obtaining first a PP-like wavefunction, along with contributions in which various PP-like pairs have been substituted with the open-shell entities. Again, the energetic relevance of the latter will determine the extent of complexification.

Further insight may be gained by comparing cRHF and (real-orbital) UHF. UHF orbitals can also be transformed to become concisely related to restricted orbitals,[101] and we will employ the same notation:

$$\begin{aligned} \xi_j^- &= \cos(\theta_j)\eta_j - \sin(\theta_j)\eta_{\hat{j}} \\ \xi_j^+ &= \cos(\theta_j)\eta_j + \sin(\theta_j)\eta_{\hat{j}}. \end{aligned} \tag{19}$$

The UHF wavefunction is an antisymmetrized product of the various $\xi_j^-\xi_j^+\alpha\beta$. In each pair, we may expand out this orbital product, obtaining Π_j, i.e. a PP-like term identical to that found in cRHF, plus

$$\Omega_j^{(\mathrm{UHF})} = \sin(\theta_j)\cos(\theta_j)(\eta_j\eta_{\hat{j}} - \eta_{\hat{j}}\eta_j). \tag{20}$$

Instead of an open-shell singlet term, we have a triplet contribution, i.e. spin-symmetry breaking. The driving force for unrestriction thus includes that for complexification in cRHF, i.e. the PP-like contributions. But, the triplet-based components are generally - often significantly - lower in energy than their cRHF singlet counterparts, and hence polarization is observed much more often in UHF. This underlies UHF's historical preponderance, as compared to cRHF.

C. Detailing the cRHF/UHF/PP connection

Continuing our cRHF/UHF comparison, we will now explicitly analyze the energy expressions. Consider the 1-electron density matrix (1-PDM) for each of the above methods, in

the η_j basis. In this basis, the 1-PDMs are block diagonal, with 2-by-2 blocks corresponding to the electron pairs. The blocks for cRHF are

$$P_{[j]} = \begin{bmatrix} \cos^2(\theta_j) & -i\sin(\theta_j)\cos(\theta_j) \\ i\sin(\theta_j)\cos(\theta_j) & \sin^2(\theta_j) \end{bmatrix}, \tag{21}$$

where the $[j]$ notation means the j-th pair. Of course, the blocks are the same for α and β spin. For UHF, we have

$$P_{[j]}^{(\mathrm{UHF};\alpha)} = \begin{bmatrix} \cos^2(\theta_j) & -\sin(\theta_j)\cos(\theta_j) \\ -\sin(\theta_j)\cos(\theta_j) & \sin^2(\theta_j) \end{bmatrix} \tag{22}$$

and

$$P_{[j]}^{(\mathrm{UHF};\beta)} = \begin{bmatrix} \cos^2(\theta_j) & \sin(\theta_j)\cos(\theta_j) \\ \sin(\theta_j)\cos(\theta_j) & \sin^2(\theta_j) \end{bmatrix}. \tag{23}$$

For PP, we get

$$P_{[j]}^{(\mathrm{PP})} = \begin{bmatrix} \cos^2(\theta_j) & 0 \\ 0 & \sin^2(\theta_j) \end{bmatrix}. \tag{24}$$

The kinetic energy, K, is given by the trace over the 1-PDM times the η_j-basis kinetic-energy matrix. The latter is real and symmetric, so the contributions coming from the imaginary parts of the cRHF 1-PDM will cancel. Likewise, for UHF, the contributions coming from the off-diagonal 1-PDM parts will cancel because the latter change sign going from α to β. The off-diagonal parts of the PP 1-PDM are already 0, and thus, cRHF, UHF, and PP have the same form for their kinetic energies. Treating K as a function of the 1-PDM, we may summarize this result as

$$K = K(P) = K(\mathrm{diag}(P)). \tag{25}$$

In what follows, we will abbreviate the term on the far right-hand-side of this equation to simply "K", and will do the same for analogous quantities defined below.

We also see that the three methods have the same form for the total electron density, ρ. The latter is a function of the 1-PDM: it is obtained by summing over each element of the 1-PDM times the product of the two pertinent orbitals. For this, all off-diagonal terms will cancel. Analogous to the K situation, we have

$$\rho = \rho(P) = \rho(\mathrm{diag}(P)) \tag{26}$$

for all three methods. This may be used to show that the three methods have the same form for N and C, their nuclear attraction and Coulomb repulsion energies, respectively, i.e.

$$N = N(\rho) = N(\rho(\mathrm{diag}(P))) \tag{27}$$

and

$$C = C(\rho) = C(\rho(\mathrm{diag}(P))). \tag{28}$$

What remains are the exchange contribution and, in the PP case, some intra-pair correlation. The former is given by the following general expression

$$X = -\frac{1}{2} \sum_{\sigma \in \{\alpha,\beta\}} \sum_{pqrs} P^{\sigma}_{pr} P^{\sigma}_{qs} \langle pq|sr\rangle. \tag{29}$$

Given that each 1-PDM element is diagonal or off-diagonal, we can divide the exchange contributions in eq. (29), each of which involves two 1-PDM elements, into four categories. The diagonal/diagonal terms are equivalent for cRHF, UHF, and PP. The diagonal/off-diagonal terms are purely imaginary in cRHF, so they must sum to 0, which is also evident from observing that each cRHF off-diagonal element is the negative of its transposed counterpart. The terms also sum to 0 in UHF because the off-diagonal α elements are the negative of their β counterparts.

For the rest, we divide X into three terms, X', X'', and X''', where

$$\begin{aligned} X' = &-\sum_{kl} \cos^2(\theta_k)\cos^2(\theta_l)\langle kl|lk\rangle + \cos^2(\theta_k)\sin^2(\theta_l)\langle k\hat{l}|\hat{l}k\rangle \\ &+ \sin^2(\theta_k)\cos^2(\theta_l)\langle \hat{k}l|l\hat{k}\rangle + \sin^2(\theta_k)\sin^2(\theta_l)\langle \hat{k}\hat{l}|\hat{l}\hat{k}\rangle, \end{aligned} \tag{30}$$

$$X'' = -\sum_{kl} \sin(\theta_k)\cos(\theta_k)\sin(\theta_l)\cos(\theta_l)(\langle kl|\hat{l}\hat{k}\rangle + \langle \hat{k}\hat{l}|lk\rangle), \tag{31}$$

and

$$X''' = -\sum_{kl} \sin(\theta_k)\cos(\theta_k)\sin(\theta_l)\cos(\theta_l)(\langle k\hat{l}|l\hat{k}\rangle + \langle \hat{k}l|\hat{l}k\rangle) \tag{32}$$

where these summations go over the electron pairs. Then

$$E_{\mathrm{cRHF}} = K + N + C + X' - X'' + X''', \tag{33}$$

$$E_{\mathrm{UHF}} = K + N + C + X' + X'' + X''', \tag{34}$$

and

$$E_{\mathrm{PP}} = K + N + C + X' + E_c, \tag{35}$$

where E_c is the intrapair electron correlation, and, for simplicity, we have omitted the nuclear repulsion energy.

We summarize the preceding results as follows. 1) In cRHF and UHF, the exchange energy may be simplified somewhat, namely, it may be decomposed into PP exchange plus some relatively straightforward "off-diagonal" terms. 2) In essence, cRHF and UHF differ only in exchange. 3) cRHF (and UHF, although it is less relevant to this paper) has a clear relationship to the PP method. The balance between the pertinent PP and open-shell-singlet terms determines cRHF's relevance. In at least some of the situations in which a gainful compromise is found, problems that are formally MR in the RHF picture may still be treated with a single-reference approach, using cRHF. We will further investigate this with some molecular examples in the next section. For these purposes, we have written an efficient cRHF implementation in the Q-Chem program,[102] which we will now describe.

D. cRHF Computational Implementation

As discussed above, all cRHF energy components besides the exchange are functions of the real part of the 1-PDM. These components can thus be evaluated (in the atomic-orbital (AO) basis) with existing RHF-type code. The exchange boils down to 4-center AO integrals, and this fact allows us to evaluate the energy and Fock matrix for cRHF by feeding the imaginary component of the 1-PDM into the existing integral generation and contraction technology of Q-Chem. Therefore the overall scaling of cRHF is the same as RHF, albeit with a slightly larger prefactor (double the number of floating point operations for the contractions). To facilitate and optimize matrix operations with complex numbers, we utilize the Armadillo linear algebra library[103] throughout our implementation. cRHF is one option in a Q-Chem library consisting of a polymorphic orbital class with derived types: RHF, ROHF, cRHF, etc., containing the methods which act on the orbitals. These orbital classes couple to a polymorphic nonlinear optimizer class with derived types: steepest descent, direct inversion of the iterative subspace (DIIS),[104,105] Broyden-Fletcher-Goldfarb-Shanno(BFGS),[106] etc. which calls methods overridden in the derived orbital classes and provides a uniform interface. For cRHF, the methods necessary to use both DIIS or Geometric Direct Minimization[107] have been implemented and were used in the examples presented below.

GDM is a form of Quasi-Newton method and thus relies on differential geometry, but it should be noted here that the energy of cRHF is not a holomorphic function. This implies that cRHF does not have a derivative in the analysis sense, but we must instead use Wirtinger calculus in order to optimize these orbitals. Wirtinger calculus simply involves treating both the real and imaginary components of a complex number or vector as separate real numbers or vectors, mapping the space of $\mathbb{C}^n$ to $\mathbb{R}^{2n}$. This allows us to reuse all the same optimizers from real-orbital code without modification other than passing vectors of double the length.

The Q-Chem library above also provides an interface for computing the stability of self-consistent field solutions within their own orbital space and outside of that space as per Seeger.[80] All forms of instability are provided within this library, e.g. RHF to UHF, RHF to cRHF, cRHF to cUHF, etc. To do this we compute the lowest eigenvalue and eigenvector of the orbital Hessian matrix:

$$\frac{\partial^2 E}{\partial \chi \partial \chi} = \begin{pmatrix} A & B \\ B^* & A^* \end{pmatrix}, \tag{36}$$

$$A_{ia,jb} = (\varepsilon_a - \varepsilon_i)\delta_{ij}^{ab} + \langle aj||ib\rangle, \tag{37}$$

$$B_{ia,jb} = \langle ab||ij\rangle, \tag{38}$$

where i and j are occupied orbitals and a and b are unoccupied orbitals. The full Hessian matrix has dimensions $2OV$ where O is the size of the occupied space and V the size of the virtual space, and as such, diagonalization of this matrix scales as $\mathcal{O}\left(O^3V^3\right)$. Transformation of the 4-center AO integrals to the molecular orbital basis for computing A and B scales as $\mathcal{O}\left(N^5\right)$ where N is the size of the AO basis. To avoid both of these potential computational bottlenecks and because we only need the lowest eigenpair to test stability, we use the Davidson algorithm,[108] which only requires products of the matrix (for which one wants the eigenvalues) with trial vectors. Computing the product of the Hessian with a trial vector in the AO basis scales as $\mathcal{O}\left(N^3\right)$, which is the same as building the Fock matrix and thus doesn't limit the systems for which stability analysis may be performed. When possible we exploit the symmetry of the problem, that is we may spin-adapt the search or remove spin-flip blocks entirely. When analyzing the stability of a given solution, if we find a negative eigenvalue (an instability), we perform a short line search downward along that direction and restart the SCF calculation starting from this point. This may be repeated at the user's request until a stable solution is found.

III. CALCULATIONS

A. Prelimary Comments

Unless otherwise noted, we used the cc-pVDZ[109] basis for all results in this section. For the upcoming examples, we report HF, Moller Plesset Second Order Perturbation Theory (MP2), DFT (BLYP[110,111] and B3LYP[112,113] functionals), and Coupled Cluster Singles Doubles[114] with Perturbative Triples[115] (CCSD(T)) results, all computed with Q-Chem.[102] These calculations were benchmarked with various "high-accuracy" methods, depending on the example system: Full Configuration Interaction (FCI), multireference MP2[116,117] (MRMP2), and MR Configuration Interaction Singles Doubles[118–120] with Davidson Correction[121] (MR-CISD+Q), with the latter two being based on Complete Active Space Self Consistent Field (CASSCF).[122–129] All of the benchmark computations were done with GAMESS.[130] We will use (m,n) to denote a m electrons in n orbitals active space (AS). We used Gnuplot[131] for all data plots.

We note that for each of the upcoming examples, results for some of the above methods (except cRHF) exist in the literature. It is important that cRHF be assessed alongside the results of standard methods, and so we have included the latter in each case below. In the interest of coherence, we used our own computations, except for some of the data used in Fig. 3 as stated below.

We will now generalize the above O_2 discourse to obtain a qualitative template for the forthcoming examples. We now assume ϕ_1 and ϕ_2 are real frontier orbitals and, as before, that u_c, the "core" wave function, is a product of doubly occupied real orbitals. The (2,2) AS associated with the frontier orbitals is spanned by the following configurations

$$\begin{aligned}
\Psi_{\mathrm{S0}} &\sim u_c(c_1\phi_1\phi_1 - c_2\phi_2\phi_2) \\
\Psi_{\mathrm{S1}} &\sim u_c(\phi_1\phi_2 + \phi_2\phi_1) \\
\Psi_{\mathrm{S2}} &\sim u_c(c_2\phi_1\phi_1 + c_1\phi_2\phi_2) \\
\Psi_{\mathrm{T}} &\sim u_c(\phi_1\phi_2 - \phi_2\phi_1),
\end{aligned} \tag{39}$$

where S0, S1, and S2 are singlets, labelled as per convention according to their typical energy ordering, T is a triplet, and c_1 and c_2 are positive scalars. If ϕ_1 and ϕ_2 are of different symmetry in an Abelian point group, a situation typifying the below examples,

then for a suitable choice of c_1 (and hence c_2), the above configurations diagonalize the (2,2) AS Hamiltonian. In each example below, each of these configurations dominates the expansion for a different exact state. We will use the same labels (S0, S1, S2, T) for these exact states, even if their energy ordering fluctuates (e.g. S1 drops below S0).

In each of the upcoming chemical examples, the system develops MR character in some relevant part of the potential energy surface (PES). This "MR region" contains at least one geometry where $c_1 = c_2$, i.e. a point of maximum MR character. Somewhere in the vicinity of this point we observe the following:

(a) RHF: two degenerate solutions, whose energies cross in the polyatomic case. This is because $c_1 = c_2$ implies degeneracy in the configurations $u_c\phi_1\phi_1$ and $u_c\phi_2\phi_2$, and likewise for the corresponding RHF solutions. Moving through the crossing, the HOMO switches from ϕ_1 to ϕ_2. At the crossing point, both $u_c\phi_1\phi_1$ and $u_c\phi_2\phi_2$ are equal-weighted combinations of Ψ_{S0} and Ψ_{S2} (c.f. eq. (4)). Accordingly, for the RHF-based data, we will primarily be interested in the S0 and S2 high-accuracy benchmarks. The same goes for the RDFT data.

(b) cRHF: maximum complexification in the frontier-orbital pair, i.e. the HOMO becomes $\phi_1 - i\phi_2$. The wavefunction is then an equal-weighted combination of Ψ_{S0} and Ψ_{S1} (c.f. eq. (7)). Accordingly, for the cRHF-based data, we will primarily be interested in the S0 and S1 high-accuracy benchmarks, although S2 is still relevant for geometries with partial complexification.

(c) UHF: spin polarization largely confined to the frontier-orbital pair, but maximal within that pair. We distinguish two ways that this can occur. For the first way, which we will call "U0", the α and β orbitals become $\mu_\alpha = \phi_1 - \phi_2$ and $\mu_\beta = \phi_1 + \phi_2$, respectively. Then $u_c\mu_\alpha\mu_\beta$ is an equal-weighted combination of Ψ_{S0} and Ψ_{T}. For the second way, which we will call "U1", the α and β orbitals become $\mu_\alpha = \phi_1$ and $\mu_\beta = \phi_2$, respectively. Then $u_c\mu_\alpha\mu_\beta$ is an equal-weighted combination of Ψ_{S1} and Ψ_{T}. In either scenario, the unrestricted wave function has a $\langle \mathbf{S}^2 \rangle$ value of 1, where $\mathbf{S}$ is the total-spin operator. For each example below, one of U0 or U1 ensues: if S0 (S1) is the ground state singlet, then U0 (U1) is observed. Accordingly, for the UHF-based data, we will primarily be interested in the S0, S1, and T high-accuracy benchmarks. The same goes for UDFT.

B. singlet O_2

We would now like to complete our above O_2 example with some realistic calculations. As for the above template, ϕ_1 and ϕ_2 are here of Π_g symmetry. If we select π_x^* and π_y^* for these two orbitals, then they have symmetry B_{2g} and B_{3g}, respectively, for the D_{2h} point group oriented along those axes. Every geometry of this molecule is a point of maximum MR character in the frontier-orbital pair.

RHF and cRHF results are given in Fig. 1. Around the equilibrium geometry, the cRHF orbitals and wavefunction are $D_{\infty h}$ symmetric, in line with our comments in the Introduction. In this region, RHF exhibits a subtle kind of SB, in contrast to our qualitative discussion above. This is because double occupation of e.g. π_x^*, which results in the SB shown in eq. (4), causes a polarization in the eq. (1) "core" upon optimization. This leads to small δ contaminations in the σ orbitals, and the π_x and π_y orbitals no longer being degenerate nor exactly related by a rotation. D_{2h} symmetry is preserved, however. These effects are analogous to unrestricted-calculations phenomena where small spin polarizations in low-energy orbitals result from larger spin polarizations in the frontier orbitals.

It is interesting that cRHF does not give a bound curve (i.e. relative to O atoms), as may be seen in Fig. 1. As the bond is stretched, D_{2h}-symmetry violating solutions break away from the symmetric ones in both RHF and cRHF. These "new" solutions break inversion symmetry and exhibit localized orbitals. This is similar to what is observed in RHF for N_2.[65,132,133] We will note in passing that N_2 also has a cRHF solution for stretched bond lengths, but will not further discuss it here. The O_2 SB cRHF wavefunction has significant complexification in two pairs, while for the symmetric solution this occurs in just one pair.

In Fig. 2, we show real and complex-orbital MP2 (RMP2 and cRMP2, respectively) results. Included are MRCISD+Q results based on (16,10) CASSCF. cRMP2 is significantly closer to the MR results than is RMP2. The energies based on the symmetric HF solutions "turn over", as usual for MP2 in bond breaking, while the SB results show a singularity at the onset of SB and quickly rising energies. This is also observed in N_2 and it is due to the orbital localization, which causes the SB HF wavefunctions to have a low overlap with the ground state. In other words, the SB MP2 results are predominantly approximating excited states in the bond breaking region. This makes it clear that cRHF cannot generally skirt the RHF SB problem.

Also in Fig. 2, we show RCCSD(T) numbers. In absolute energy, these are rather close to those of cRMP2 near the equilibrium geometry. This is an intriguing outcome. On one hand, the MR character of the $^1\Delta_g$ state is, in a sense, confined to the π^* space, which contains only two electrons for this system. CCSD is exact for two-electron systems, and would be exact if the correlation treatment were confined to the associated (2,2) AS, and we might therefore be inclined to think that RCCSD(T) would be chemically accurate here. On the other hand, the reference determinant is contaminated by excited states approximately as given in eq. (4). In cases like this, it is important to appreciate that the quality of the CCSD method is determined not only by its cluster wavefunction, but also by the reference determinant and the substituted determinants derived from it, which underlie the projection equations and thereby the energy. If the substituted determinants also break symmetry, as is the case here, their projection equations may force the RCCSD wave function to do likewise.

To further probe this point, we have done additional RCCSD(T) calculations with larger bases, and, in Fig. 3, we compare the results to highly accurate full-valence MRCISD+Q data for the $^1\Delta_g$ and $^1\Sigma_g^+$ states. We also include RB3LYP results to show that standard DFT methods, as represented by this, the likely most popular functional, are essentially in the same boat as CC for this example. UCCSD(T) and UB3LYP were used for the (triplet) O atom to compute relative energies.

The MR numbers were taken from the Supporting Information of ref. 134. In that work, the data was obtained by extrapolating to the complete basis set (CBS) limit. Likewise, we performed a CBS extrapolation following the protocol suggested in references 135 and 136. For this, we computed RCCSD(T) energies with the frozen-core approximation and with the aug-cc-pVTZ and aug-cc-pVQZ bases,[137] and then fit the functions $E_{\mathrm{HF},X} = E_{\mathrm{HF,lim}} + Be^{-1.63X}$ and $E_{\mathrm{CE},X} = E_{\mathrm{CE,lim}} + BX^{-3}$ to the RHF and correlation energies (CE), respectively, where $X = 3$ or $X = 4$ for aug-cc-pVTZ and aug-cc-pVQZ, respectively.

We found that the RB3LYP binding energy changed by less than a tenth of a kcal/mol when going from aug-cc-pVQZ to aug-cc-pV5Z, and as such we concluded there was no need for a CBS extrapolation for this method, i.e. the RB3LYP data in Fig. 3 are those computed with aug-cc-pVQZ.

The main observation in Fig. 3 is that, near equilibrium, RCCSD(T) is quite close to halfway in between the $^1\Delta_g$ and $^1\Sigma_g^+$ energies. This is very consistent with eq. (4), and

implies that RCCSD(T) is not able to improve the SB situation of RHF. The RB3LYP energy appears to be biased towards that of the $^1\Sigma_g^+$ state, although we note that the RB3LYP relative energy is fairly close to that of RCCSD(T) if the former is computed using the restricted open-shell B3LYP energy of the O atom. In any case, RB3LYP is far from chemically accurate for either of the pertinent exact states. Although we have not included RBLYP data in this plot, we will refer to it in the next subsection.

As spoken of in the Introduction, one may be inclined to turn to unrestricted methods at this point. Since the underlying states of interest are singlet spin, this entails doing UHF (or UDFT) with an equal number of α and β electrons. We have reported such calculations in an earlier paper,[2] and there, we compared the results with the same high-accuracy MR data.

Around equilibrium, the UHF and UDFT orbitals adhere to the above template. In this case, the S0-S1 degeneracy means that U0 and U1 are energetically equivalent. The UCCSD(T) and UB3LYP energies are thusly complicit: they lie in between the MR $^1\Delta_g$ and $^3\Sigma_g^-$ energies. Thus, in this case, unrestricted methods fare no better than their restricted counterparts.

Finally, we note that the cRMP2 binding energy, as computed with ROHF/MP2 for the O atom, is about 10 kcal/mol lower than that of MRCISD+Q at both the cc-pVDZ and aug-cc-pVQZ levels. This does not appear to be a fundamental problem, because cRMP2/cc-pVDZ is still noticeably above MRCISD+Q in absolute energy. This issue evidently relates to a poor MP2 energy for the O atom. We expect an accurate binding energy at the cRCCSD(T) level; the above discussion implies that RCCSD(T)'s Δ_g and Σ_g^+ components are likely to be individually accurate, and cRHF will effect the removal of the latter contaminant.

C. A Pople-type Example: BeH_2

Pople's paper,[75] although highly insightful, did not present a genuine molecular system. For our initial exploration in this setting, we would like to use a very simple instance of such a system, whose properties are similar to the hypothesis of Pople's abstract model. For this, we chose BeH_2, a common example in the MR literature.[138–149] A typical PES is defined by

the following cartesian coordinates:

$$\begin{aligned} &\mathrm{Be} : (0, 0, 0) \\ &\mathrm{H} : (x, 1.344 - 0.46x, 0) \\ &\mathrm{H} : (x, -1.344 + 0.46x, 0), \end{aligned} \tag{40}$$

where the units here are Å. At $x = 0$, we have linear BeH_2, and as x is increased, the hydrogen atoms are pulled laterally away from the beryllium atom, and closer to one another, reaching Be + H_2 at around $x = 2.1$ (see Fig. 1 in ref. 141). For all $x > 0$, the geometries have C_{2v} symmetry.

This PES is of MR interest because the dominant electron configuration of the ground state at $x = 0$ is $(1a_1)^2(2a_1)^2(1b_2)^2$, but it is $(1a_1)^2(2a_1)^2(3a_1)^2$ at $x = 2.1$. Applying our above template, ϕ_1 and ϕ_2 have B_2 and A_1 symmetry, respectively, and S0, S1, S2, and T have A_1, B_2, A_1, and B_2 symmetry, respectively. We expect an RHF solution crossing, leaving a singularity in the RHF energy.

In Fig. 4, we plot RHF and cRHF energies as a function of x. The results are essentially as expected, with cRHF "smoothing" over RHF. Naturally, this is a desirable outcome, but further inspection is in order because, in contrast to the O_2 case, the PP-like and open-shell pieces of cRHF in BeH_2 are of different symmetry. To address this, in Fig. 5, we plot RMP2 and cRMP2 along with accurate S0, S1, and S2 curves as per the template. Each energy in this plot is shown relative to the pertinent method's energy for S0 at $x = 0$. We chose this geometry/state combination as a reference because all methods considered are well behaved there, i.e. it is not SC.

Notably, S1 becomes the singlet ground state for intermediate x values. In addition, RMP2 and cRMP2 are qualitatively consistent with the "contaminated" nature of their reference determinants as laid out in the template. The RMP2 crossing-point energy is shifted up from that of S0, towards S2 as expected. It is actually closer to S2 than S0 at this point. This may be due to RMP2's poor quality in the Be + H_2 region, which itself is due to RMP2's poor treatment of certain $ss \rightarrow pp$ correlations the Beryllium atom. If this were somehow improved such that the RMP2 curve for the right RHF solution is simply shifted downward, the crossing-point energy would end up being close to midway between S0 and S2.

We include RBLYP, RB3LYP, and RCCSD(T) data in the Supplementary Material.[201]

The RBLYP and RB3LYP results are very similar to those of RMP2, with crossing-point energies slightly shifted down and to the right, but with the same inaccuracy in the Be + H_2 region. For most x values, RCCSD(T) is chemically accurate. The left and right RCCSD(T) curves each "turn over" and head downward at a very fast rate when moving to the right and left of the RHF crossing point, respectively. Nevertheless, if we select the best of the two energies at each x value, it never varies from the accurate S0 curve by more than 2 kcal/mol. A similar result was found several years ago using RCCSD.[138] This likely represents a situation where the system is small enough (4 valence electrons) that CCSD(T) can significantly overcome the effects of a poor reference determinant.

The cRMP2 energy is qualitatively consistent with an S0-S1 mixture, again as per the template. To the right of $x = 1.5$, at which point the S0 curve maximizes, cRMP2 continues to rise temporarily, concomitant with S1's continuing rise. This makes cRMP2 less symmetric looking compared to S0 in this region, and shifts the cRMP2 maximum to the right of that of RMP2. That the cRMP2 relative energy does not lie in between those of S0 and S1 may again be related to RMP2's poor quality for Be atom, i.e. moving to the right cRMP2 has to join with an "upshifted" RMP2 energy.

We turn to unrestricted methods. First, ab initio results are plotted in Fig. 6, along with accurate S0, S1, and T curves as per the template. We first observe that in the intermediate region, T is the overall ground state. The underlying UHF data, plotted in the Supplementary Material,[201] consists of three solutions. The first one predominates between $x = 0$ and around $x = 1.2$, at which point the second solution crosses the first and predominates until around $x = 1.65$, whereupon it crosses with the third solution, which predominates thereafter. The second crossing persists in the UMP2 and UCCSD(T) data, while the first UHF crossing becomes a bona fide discontinuity. This somewhat unusual behavior is due to S1 and T dropping below S0 in the intermediate region. The second UHF solution corresponds to a U1 situation as described above, whereas the first and third solutions correspond to a U0 situation (if they are allowed to "continue" into the intermediate region). Here, the UMP2 energy is very close to lying midway between those of S1 and T, while UCCSD(T) is somewhat closer to T.

UDFT results are plotted in Fig. 7. First, we see that UBLYP and UB3LYP each produce only one curve with no crossings, something we have carefully checked by performing calculations at numerous x values in the two relevant regions. Instead of crossings, there

exist bifurcations at the two relevant geometries, and on the lower curve each functional is gradually transitioning from S0/T-like constituents to S1/T-like constituents. This result, although perhaps seemingly advantageous, is actually unphysical because the underlying exact states cross.

UB3LYP resembles UCCSD(T) in the intermediate region, while UBLYP is rather close to the accurate T curve. The latter result is quite interesting, given the SB in its underlying determinant. To exclude possible basis set effects here, which are generally relevant for DFT calculations with small basis sets, we computed UBLYP/cc-pVQZ[109] energies at $x = 0$ and $x = 1.4$, and benchmarked this data with full-valence MRMP2/cc-pVQZ calculations for S0, S1, and T. The results corroborated the cc-pVDZ data. If this outcome is a legitimate one, it certainly would be counted as a success for BLYP. But, there is a reasonable amount of doubt for this, as shown with the following counterpoint.

For O_2 at bond length 1.21 Å, the RBLYP/aug-cc-pVQZ binding energy is 99.4 kcal/mol, in good agreement with the MR data for $^1\Delta_g$ in Fig. 3. This might make it seem like RBLYP is overcoming the SB of its auxiliary determinant, which has been qualitatively described in the above template. Indeed, this situation is very similar to what we are observing just above for BeH_2. However, for the triplet, UBLYP/aug-cc-pVQZ gives a binding energy of 135.8 kcal/mol, which is about 15 kcal/mol too high.[134] The above-mentioned agreement regarding the RBLYP energy for O_2 is therefore spurious. This result isn't unfamiliar; there are known examples of appreciable BLYP overbinding,[150–153] a notable one being the chromium dimer.[154,155] A further indication that this may also be occuring for BeH_2 is that the UBLYP relative energy is significantly below those of S0 and T where the latter curves cross near $x = 1.2$. In other words, if UBLYP is demonstrably overbound there, couldn't this also be the case around $x = 1.4$? One might obtain some further clues for this by exploring the more general BeH_2 PES (i.e. geometries not found along the selected C_{2v} cut), but we will not attempt that here.

D. A Woodward-Hoffmann Violating Reaction

The BeH_2 model, although providing a good conceptual testing ground, largely functions as a prototype. We have endeavored to determine which general and chemically relevant molecular classes would benefit from cRHF.

One promising area is found in the various organic reactions to which the WoodwardHoffmann (WH) rules have been famously applied.[156] In our perspective, the WH rules appear to be closely related to the general idea that reactions are allowed if and only if the associated (RHF) occupied space transitions smoothly between reactant and product. In other words, the latter property is thought to correlate well with low energy barriers. As such, reactive processes entailing RHF frontier-orbital interchanges and/or associated with multiple RHF solutions and the associated energetic singularities would generally be (thermally) forbidden. Naively, this seems detrimental to cRHF's relevance in this context.

There are (at least) two significant contradictions to this assumption: First, these thermally forbidden reactions often still proceed photochemically, via excited states that eventually reconnect with the ground state PES, and thereby to the products, via conical intersections (CI). In a prototypical situation, the excited state is dominated by an open-shell configuration obtained as a single HOMO-LUMO excitation from the ground-state determinant. cRHF is thus of interest for such cases. Unsurprisingly, the situation in practice is more complicated (see e.g. the literature cited below for butadiene), but we still expect open-shell terms being sufficiently low to admit a distinct cRHF solution in the general vicinity of the CI. As to the second contradiction, for some reactions that are technically forbidden by the WH rules, the barriers of the ground state PES's are low enough to grant a measure of chemical relevance. These are the WH violating (WHV) reactions.[157–166]

Initially, we were inclined to look for cRHF solutions in the 1,3-butadiene ring closure to form cyclobutene, an archetype reaction of WH theory. The thermal reaction proceeds through a conrotatory mechanism, in which the hydrogen atoms on the two terminal carbon atoms rotate in the same direction as the carbon atoms come closer to each other. Throughout this PES, RHF is well behaved. Conversely, a (ground-state) disrotatory process, wherein the pertinent hydrogen atoms rotate in opposite directions, must involve a frontier-orbital interchange and therefore would be WH forbidden. Even if its barrier were high, it might still be of academic cRHF interest. But even this turns out to be extraneous: studies employing MR wave functions have found no legitimate (ground-state) transition state (TS), i.e. first-order saddle point, consistent with a concerted disrotatory PES.[167–169] Thus, practical investigations of disrotatory processes for this system are effectively confined to the excited state/CI realm. The associated photochemical reaction is well known and tractable. It involves multiple CI's and is generally intricate.[170–176] But, for reasons

discussed in the next subsection, we have chosen not to pursue the CI/cRHF connection in WH reactions in this paper.

Things are different for a modified version of this reaction. Consider the ring opening (just the reverse of closure) of *cis*-bicyclo[2.1.0]pent-2-ene (**1**) to form *cis*,*cis*-cyclopenta-1,3-diene (**2**). These structures are analogs of cyclobutene and 1,3-butadiene, respectively (see Fig. 8). Theoretical ground-state studies[177,178] have shown that the added carbon atom, which starts off in a cyclopropyl group, serves to force the molecule into a ring-opening disrotatory motion that entails a TS.

To test cRHF on this system, we need to obtain the geometries of its PES. We aim for the simplest level of theory that is qualitatively correct. The σ-bond framework stays roughly intact throughout the reaction, while the π framework clearly gets rearranged. Before performing calculations, it is difficult to predict with high confidence whether the essence of this reaction is limited to the expected HOMO/LUMO interchange, which could be effectively modeled with a (2,2) AS, or if it will require a full 4-electron π space treatment. Accordingly, we proceeded with state-specific (SS) CASSCF(4,4).

As a guess geometry, we used the TS geometry computed in ref. 178. This guess geometry has C_s symmetry, and we note that the reactant and product have a common (i.e. conserved) C_s axis, which, for example, bisects the cyclobutene group of the reactant, passing through the cyclopropyl carbon atom. Thus this symmetry constraint was used when computing the various reaction-path geometries. Using this guess geometry, we did a TS calculation at the CAS(4,4) level. With a vibrational analysis, we verified that the obtained geometry is a true TS, and have included its coordinates in the Supplementary Material.[201]

Starting from the TS geometry, we performed SS CAS(4,4) Intrinsic Reaction Coordinate (IRC) calculations,[179–181] which gradually perturb the starting geometry into two energy minima that are connected via the TS. We verified that the two obtained minima correspond to the desired reactant and product. The reaction path is quantified by a variable, S_{total}, which measures the distance traveled from the TS, and has units $\sqrt{\text{amu}}$ * Bohr radius.[182] The details of S_{total} are not essential for our present purposes; we only need to know that the TS corresponds to $S_{total} = 0$, while the leftmost and rightmost values in the forthcoming plots correspond to reactant and product, respectively. We used the IRC geometries for all subsequently discussed calculations on this system.

Deciding on a level of theory to use for benchmarking the pertinent approximations is

slightly complicated. MRMP2 based on CASSCF is in principle adequate here. However, since we expect complexification in at least one pair, we expect (at least) 3 singlet states to be relevant to RHF and cRHF in the MR region of the PES, while the associated triplet should be additionally relevant to UHF. As per our above template, we need to include such excited states in the benchmarking. The use of SS ground-state CAS orbitals for excited states is not advisable. Also somewhat dubious are separate orbital opimizations for each excited state; for example, we were unable to converge the 2nd excited singlet this way. State averaging (SA) is the more reliable approach here, but even this is a little tricky for the (4,4) AS. This is because the required 4 states mentioned just above are not always the lowest four states to be found at any given geometry along the PES, making them difficult to track.

To get around this issue, we looked at natural-orbital occupation numbers at the geometry exhibiting the highest degree of MR character, which, at the SS CAS(4,4) level, occurs around $S_{total} = 0.7$. At this geometry, the occupation numbers are 1.89, 1.04, 0.96, 0.11, which is close to 2,1,1,0, meaning that qualitatively, this reaction can be correctly modeled by a (2,2) AS after all. Additionally, at $S_{total} = 0.1$, the highest occupied and lowest unoccupied natural orbitals have symmetry A′ and A″, respectively, while the ordering is reversed at $S_{total} = 1.0$. This frontier-orbital interchange suggests an RHF solution crossing, and bodes well for a distinct cRHF solution. Thus, applying our template, ϕ_1 and ϕ_2 have these two symmetries, and S0, S1, S2, and T have A′, A″, A′, and A″ symmetry, respectively.

The (2,2) AS's dimension is only 4, and it contains the 4 states of greatest interest, so here, SA is straightforward. Therefore, along the reaction path, we optimized orbitals by averaging over the lone triplet and 3 singlet energies in CAS(2,2), and used these orbitals to perform MRMP2 calculations. This approach is further supported by qualitative similarity between its PES for the ground state and that obtained using MRMP2 based on SS CAS(4,4), which is shown in the Supplementary Material.[201] The two curves have very similar reactant-TS barriers, but the product-TS barrier for (4,4) is larger. The (2,2)-based numbers will thus serve as our benchmark. We note that the CAS(2,2) singlet energies do not cross at any point along the PES, i.e. they are always in accord with the S0-S1-S2 labelling. This is not the case for MRMP2, as we will see.

We computed RHF and cRHF along the IRC. Sure enough, as Fig. 9 shows, an RHF singularity occurs, which is smoothed over by cRHF. The associated MP2 energies are also

shown in Fig. 9. For these and all forthcoming plots for this system, each energy is shown relative to that of the respective method's approximation for the ground state at the reactant geometry.

To assess the MP2 results, consider the MRMP2 benchmark data for the 3 singlets shown in Fig. 10. The cRMP2 curve is not included in this plot because on this scale, it appears scantly different from that of RMP2. The MP2 energies are visibly consistent with our template, with the benchmark S0 and S2 curves resembling "adiabatic" counterparts to the "diabatic" RMP2 curves. Curiously, S2 drops below S1 in this region, in opposition to the CAS result. This MRMP2 observation is consistent with the cRMP2 curve, which veers upwards from the RMP2 curve in the complexification region, while the CAS energy ordering is consistent with cRHF dropping below RHF there. This is to be compared with the BeH_2 case, where the cRMP2 barrier height is more accurate due to that system's S0 and S1 states being much closer in energy in the MR region.

These observations also explain why the RMP2 crossing point lies to the right of the S0 barrier. The two RMP2 energies do not become degenerate until the maximal MR point. Although the exact location of this point varies slightly between the various methods, it invariably occurs to the right of $S_{total} = 0$, hence the right-shifted "barrier".

The RBLYP and RB3LYP curves are similar to those for RMP2, so we include them in the Supplementary Material.[201] We have included RCCSD(T) results in Fig. 10. The RCCSD(T) barrier height is a significant improvement over that of RMP2. In contrast to the O_2 results, here RCCSD(T) is found below the midpoint between the ground state and pertinent excited state. However, the singularity remains, although each RCCSD(T) curve does appear to exhibit a maximum, i.e. a barrier.

We show unrestricted results in Fig. 11. The UHF wave function breaks spin symmetry at all points shown, with $\langle \mathbf{S}^2 \rangle$ values ranging from 0.19 to 1.26 to 0.40 at the reactant, MR, and product geometries, respectively. Spin polarization occurs in UBLYP in the S_{total} interval [-1.2,1.6], and in UB3LYP in the interval [-1.7,1.9]. These functionals give maximal determinantal $\langle \mathbf{S}^2 \rangle$ values of 1.02 and 1.04, respectively, each of these numbers occuring essentially at the maximal MR point. These considerations, along with those discussed above for the restricted results, indicate that the unrestricted results fit the U0 designation.

Near the maximal MR point, the UCCSD(T) energy is in between those of S0 and T. This is not the case for the UDFT energies, but it would be if we had used the product geometry

to define the relative energies. The product is non-SC and closed-shell, so it would also be a valid reference point; indeed, switching to it would not alter our UCCSD(T) observation. There is another reason that the closeness of the UDFT and S0 energies at the maximal MR point might still be consistent with admixture: the SS (4,4) MRMP2 T energy, shown in the Supplementary Material,[201] is very close to that of S0 at that geometry.

Compared to MRMP2 S0, each unrestricted method exhibits a left-shifted and raised barrier. Both of these attributes are consistent with triplet-energy admixture: to the right of $S_{total} = 0$, both the S0 and T benchmark energies are going down, as are all of the unrestricted energies, and to the left of $S_{total} = 0$, the T energy rises more quickly than the S0 energy falls, while correspondingly, the unrestricted energies rise temporarily to a maximum. Thus, the unrestricted data is generally consistent with the template.

The reduced range of spin polarization in the DFT results is consistent with the behavior of MRMP2 T, which is low lying only in the general MR region; the DFT functionals have enough correlation to "see" that there is no point to mixing in a triplet contribution to the energy outside this region. Accordingly, UHF is short sighted in its SB extent, a problem clearly unmasked in the UMP2 results.

E. Symmetry-driven Conical Intersection

As stated above, the combination of PP-like and open-shell terms inherent in cRHF (c.f. eq. (15)) recommends its usage for CI's whose two (or more) associated states are dominated by such terms. We were interested in the CI's found in the ring opening of cyclobutene, and we particularly wanted to study DNA bases and related molecules, which exhibit CI's that appear to fit this description, especially those between the ground state and π-to-π^* excited states.[183–189] Some of these cited papers report CI geometries as computed with MR methods with relatively large AS's. On a handful of these geometries, we ran some exploratory calculations, but each one showed that RHF was stable to complexification. Upon further contemplation, this isn't very surprising: it is quite possible that here, as in the above examples, complexification is limited to a small geometric window, which would be unlikely to contain the literature geometries as these were computed at a rather different level of theory. The best we can hope for here is qualitatively similiarity. For these systems, the CI's do not occur at "intuitive" geometries, so their locations must be computed. A

search for "cRHF geometries" must likewise be computational. Our cRHF codes are not presently equipped for this.

As a result of these difficulties, we shifted our focus to CIs whose geometries are intuitive, i.e. those driven by spatial symmetry. For this paper, we have chosen $C_5H_5^+$, the cyclopentadienyl cation. This system has a CI in its singlet ground state at the pentagonal (D_{5h}) geometry, making it a Jahn-Teller system: the molecule distorts to energetically preferable C_{2v} structures.[190–197] The latter comprise two unique geometry stationary points: one dienylic and one allylic structure, as depicted in Fig. 12. As a model for these processes, we have selected a one-parameter C_{2v} cut of the PES. Each geometry along this cut is planar, and each is obtained by placing a carbon atom at position (0,1.208) (in Å) and a hydrogen atom at (0,2.288), and successively rotating these positions by the angles given in Fig. 13 to obtain the positions of the remaining atoms. With these starting positions, the C-H bond lengths are always 1.08 Å, while C-C bond lengths are 1.42 Å at the D_{5h} geometry. The latter occurs at $\Theta = 0$, while negative and positive Θ values correspond to perturbations in the dienylic and allylic directions, respectively. The exact geometry stationary points are not found along this cut. Computing a C_{2v} path that does contain these structures is somewhat complicated due to lack of a proper corresponding transition state (see below comments on pseudorotation), and because of some SS/SA issues to be discussed shortly. Rather, our chosen cut serves as a qualitative approximation for the distortions, with the advantage that it is simply defined.

Comparing the dienylic and allylic structures in Fig. 12, they differ by a restructuring of the π bonds, but the σ bonds stay relatively intact. This implies that the π space should contain the essential correlations. At $\Theta = -2$, the RHF π orbitals have symmetries B_1, A_2, B_1, B_1, A_2, in order of increasing energy. At $\Theta = 2$, this switches to B_1, B_1, A_2, A_2, B_1. The 2nd and 3rd orbitals in each of these sequences are the HOMO and LUMO, so, yet again, we have a PES underlied by a frontier orbital interchange. In this case, T and S1 are B_2 symmetry, while S0 and S2 are A_1.

As shown in Fig. 14, RHF calculations produce the expected result: two solutions that cross at the D_{5h} geometry. At that point, the π orbitals have symmetries A_2'', E_1'', and E_2'', in order of increasing energy. Of course, this is only approximately true in RHF, because half occupation of the degenerate E_1'' level leads to polarization and some orbital SB, as observed earlier in O_2.

At D_{5h}, the four low lying states of interest have energy orderings and symmetries

$$\begin{aligned} T &: A_2' \\ S0 &: E_2' \\ S1 &: E_2' \\ S2 &: A_1'. \end{aligned} \tag{41}$$

Because T is the ground state for our selected PES region, and because it is essentially single reference, all energies reported in this subsection were computed relative to the D_{5h} T energy. To do this properly, for each of the various methods used to approximate the excited states here, we must use a concomitant method to compute the D_{5h} T energy. For RHF, we used ROHF for T, while for cRMP2, we used ROMP2 for T, etc.

S0 and S1 are degenerate at D_{5h}, and here, the cRHF wave function has the correct E_2' symmetry. D_{5h} $C_5H_5^+$ is therefore a polyatomic analogue of O_2. More generally, cRHF smoothes the RHF singularity, as may be seen in Fig. 14.

To benchmark these results, we turn to CASSCF. The energetic closeness of the four states indicates that, once again, we ought to use some SA. This is confirmed by a SS CAS(4,5) calculation on S0 at the D_{5h} geometry; using these orbitals, the S1 energy, as computed in the same AS, is 29.6 kcal/mol higher than that of S0. Furthermore, there is a singularity in the SS-CAS S0 energy at the D_{5h} geometry, as shown in Fig. 14. This is a consequence of two solutions crossing, similar to what we have generally been observing for RHF. It demonstrates the underappreciated fact that CASSCF, like HF, is susceptible to SB problems.

We therefore proceeded to average over the 4 lowest states in CAS (4,5). In contrast to our previous example, usage of this AS entails no state reordering across the PES. We therefore include the corresponding SA CASSCF energies in Fig. 14. The SA numbers respect the S0/S1 degeneracy at D_{5h}, while providing smooth energy profiles across the distortion.

We show MP2 results in Fig. 15. The cRMP2 curve is somewhat odd. In particular, around D_{5h}, it has a curvature opposite to that of the singlet ground state. This does not seem to have a straightforward explanation. It could be that cRMP2 is producing an entirely spurious result, as it does for the symmetric solution as O_2 dissociates. Such behavior is not uncommon for HF wavefunctions that have large overlaps with multiple exact states, which is the case here, with a large overlap with S1. Alternatively, it could be that cRMP2

is exhibiting a more legitimate admixture of ground and excited state energies. If so, it would somehow be modifying the predominantly ground-state character of the cRHF energy to a predominantly excited-state "concave up" curve, perhaps even implicating S2. This evokes the shortsightedness of HF, as mentioned earlier, where the relevance of uncorrelated (excited-type) states gets overestimated. In such circumstances, it might be of interest to reoptimize the orbitals with correlation included.[198–200] For this, it may be reasonable to expect the most sigificant energy lowerings to occur at medium values of Θ, where SB and excited-state admixture is most problematic, while also expecting smaller changes at $\Theta = 0$ and for large (perhaps here unplotted) Θ values, where the ground state is more single-reference in character (in the cRHF sense). In other words, would orbital optimization reverse the curvature of cRMP2, and without much vertical shifting? In any case, cRMP2's ambiguous behavior for this system stands in contrast to what we have observed in the previous examples.

RB3LYP, RBLYP, and RCCSD(T) all produce curves essentially parallel to those of RMP2, but shifted down by 1.3, 3.8, and 6.1 kcal/mol, respectively. A plot for these data is included in the Supplementary Material.[201] RCCSD(T) is more in agreement with MRMP2 than is RMP2: RCCSD(T)'s relative energy at $\Theta = 0$ of 20.6 kcal/mol is fairly close to lying midway between the corresponding numbers for MRMP2 S0 (11.9) and MRMP2 S2 (25.5), in line with the RHF wave function having comparable overlaps with the exact S0 and S2 wave functions at this point. The parallelity between the RCCSD(T) and RMP2 curves implies that the vertical displacement between them is due to inconsistencies in how the triplet energies are computed. It may be that the RMP2/ROMP2 pairing is less compatible than is the RCCSD(T)/ROCCSD(T) one, something like what we saw earlier for O_2.

We turn to unrestricted methods. For cyclic polyenes with an even number of carbon atoms, unrestricted methods typically spin polarize such that nearest-neighbor carbon atoms have opposite spin (e.g. in the Mulliken sense). In the present odd-numbered case, the spin polarization cannot be arranged symmetrically, as there would be 3 α and 2 β spins. To identify one potential outcome of this fundamental problem, we must note that at the D_{5h} geometry, there are actually 5 possible C_{2v} point groups; for example, each group's rotation axis bisects a different carbon atom. Therefore, there are 5 equivalent dienylic structures, and likewise for the allylic structures.

The preferred transition between dienylic and allylic structures does not go through the

C_{2v} path we have been studying, but rather follows a pseudorotation in which the position of one double bond is preserved in the transition (as opposed to our C_{2v} path, where the allylic double bond is in a position different from those of the dienlyic).[191] In other words, upon pseudorotation, the C_{2v} group is switched. The above spin polarization is not conducive to this preferred transition, and we expect singularites in the UHF energy there. However, the barriers and energy gaps are very low for this process, and we therefore thought it worthy of mention but not of further examination in this paper.

Returning to our C_{2v} path, we show unrestricted results in Fig. 16. Given that S0 is the singlet ground state at all points shown, we have a U0 situation, and we thus expect unrestriction to entail a mixture between S0 and T. The UBLYP, UB3LYP, and UCCSD(T) energies are consistent with this: they are concave up and they each lie in between and are generally flatter than the S0 and T energies. The UMP2 energy is also concave up, but its position is quite high (16.5 kcal/mol at D_{5h}). To not obscure the other curves, we did not include UMP2 in the plot.

IV. DISCUSSION AND CONCLUSIONS

In this work, we have studied the largely forgotten method, restricted Hartree Fock with complex orbitals. We introduced a pairing theorem that reveals a concise connection between cRHF and RHF, wherein complexity is introduced to a doubly occupied RHF pair via an individualized virtual RHF orbital. This result was used to show that cRHF, UHF, and PP are actually quite closely related, and it is also helpful for understanding cRHF's utility and in predicting when complexification will occur. A main theme here is that the presence of a relatively low-lying open-shell singlet state is closely connected to the occurrence of a distinct cRHF solution.

We have implemented an efficient cRHF code within QChem at the same scaling as RHF. We have also included the capability to test if the solutions found are minima or saddle points via a stability analysis. This analysis has the same scaling as the SCF procedure and thus it is feasible for usage on any system for which one has cRHF solutions.

We applied cRHF to four examples. Each displayed complexification essentially within just one pair (except for O_2 upon dissociation), this pair corresponding to the frontier orbitals. We showed that the standard ground-state methods are ineffective for singlet O_2.

The latter three examples were all characterized by a frontier orbital interchange, where the LUMO drops below the HOMO and RHF solutions cross. Despite all these similarities, each of the latter 3 examples presented a fairly different context. At the points of maximum complexification, we observed: 1) for BeH_2, SB in cRHF and a small, in fact negative, S0-S1 gap (in the "exact" energies), 2) for the WHV reaction, SB in cRHF and a big S0-S1 gap, 3) for $C_5H_5^+$, no SB in cRHF and an S0-S1 degeneracy. These variations made for rather different outcomes at the cRMP2 level, a subject we will return to shortly.

We would like to point out that D_{5h} $C_5H_5^+$ is a cyclic molecule with a half-filled, doubly degenerate HOMO, so it is antiaromatic. Considering these attributes, we immediately surmise that cRHF is a useful, if not the prefered, method for antiaromatic systems. We should note that many antiaromatics, such as cyclobutadiene, differ from $C_5H_5^+$ in that they do not have degenerate singlet ground states. Nevertheless, we have confirmed that C_4H_4 indeed has a distinct cRHF solution with properties similar to what we have seen in this work.

Although the unrestricted DFT results shown in this paper were generally better than their (real) restricted counterparts, they did exhibit a particular limitation. For the most part, spin polarization in DFT is considered to be much less of a problem than it is in ab initio theory. In part, this is due to the observation that DFT functionals tend to be more resistant to spin polarization than are ab initio methods, which is generally advantageous. But, it has also been suggested that even when the level of spin polarization is significant, it is still much less of a problem in DFT. At least three of the examples considered in this work contradict this claim, each one showing evidence of triplet contamination for all unrestricted methods used, both DFT and ab initio.

Accordingly, it may be worth it to incorporate complex orbitals into restricted DFT. For one, we generally expect complexification in RDFT to correspond well with that in cRHF for the kinds of systems studied above. In addition, consider a point made in the Theory section: in the pairing representation, the off diagonal elements of the density matrix, which are imaginary, cancel out when the density is formed. In the latter 3 examples of this paper, these elements were the source of SB in cRHF, which itself was implicated in the cRMP2 inaccuracies. Thus, this observation may have significant cRDFT implications, especially for pure functionals. Nevertheless, we have to be cautious here. Upon running stability analyses on RBLYP for some geometries of the WHV reaction, we found real-to-complex instabilities

only in between $S_{total} = 0.3$ and 0.6, meaning cRBLYP will differ from RBLYP only within this gap. But the inaccuracy of RBLYP extends beyond this small range, so cRBLYP may still fall short for this system. The energetic position of the open-shell singlet excited state thus appears to be operative here. Again, this idea underlies all the complex-restricted approximations discussed in this paper. We might expect a more favorable outcome for BeH_2, with its low lying S1. In any case, experimentation with cRDFT is in order.

It seems reasonable to assert the efficacy of cRMP2 and cRCCSD(T) (and possibly cRDFT) for systems like O_2 (near equilibrium) and D_{5h} $C_5H_5^+$. For the other situations considered here, cRMP2's behavior is erratic, and cRCCSD(T)'s ability to adequately correct this is uncertain. Accordingly, perhaps the pivotal distinction of cRHF is that it can, in at least certain important cases, resolve singularities in the RHF energy. This may entail some SB, but for single-reference methods based on restricted HF, a reference determinant with this "smoothing" property may prove to be vital. It will be of significant interest to see how the new SC-inspired, hitherto RHF-based, single-reference approximations noted in the Introduction would perform in this context.

ACKNOWLEDGMENTS

This work was supported by the Director, Office of Science, Office of Basic Energy Sciences, of the U.S. Department of Energy under Contract No. DE-AC02-05CH11231. M.H.-G. is a part-owner of Q-CHEM Inc.

[1] D. W. Small and M. Head-Gordon, J. Chem. Phys. **130**, 084103 (2009).

[2] D. W. Small and M. Head-Gordon, Phys. Chem. Chem. Phys. **13**, 19285 (2011).

[3] D. W. Small, K. V. Lawler, and M. Head-Gordon, J. Chem. Theory Comput. **10**, 2027 (2014).

[4] P. A. Limacher, P. W. Ayers, P. A. Johnson, S. De Baerdemacker, D. Van Neck, and P. Bultinck, J. Chem. Theory Comput. **9**, 1394 (2013).

[5] P. A. Johnson, P. W. Ayers, P. A. Limacher, S. D. Baerdemacker, D. V. Neck, and P. Bultinck, Comp. Theor. Chem. **1003**, 101 (2013).

[6] K. Boguslawski, P. Tecmer, P. W. Ayers, P. Bultinck, S. De Baerdemacker, and D. Van Neck, Phys. Rev. B **89**, 201106 (2014).

[7] J. A. Parkhill, K. Lawler, and M. Head-Gordon, J. Chem. Phys. **130**, 084101 (2009).

[8] J. A. Parkhill and M. Head-Gordon, J. Chem. Phys. **133**, 024103 (2010).

[9] G. E. Scuseria, C. a. Jiménez-Hoyos, T. M. Henderson, K. Samanta, and J. K. Ellis, J. Chem. Phys. **135**, 124108 (2011).

[10] C. a. Jiménez-Hoyos, T. M. Henderson, T. Tsuchimochi, and G. E. Scuseria, J. Chem. Phys. **136**, 164109 (2012).

[11] T. Stein, T. M. Henderson, and G. E. Scuseria, J. Chem. Phys. **140**, 214113 (2014).

[12] R. Schutski, C. A. Jiménez-Hoyos, and G. E. Scuseria, J. Chem. Phys. **140**, 204101 (2014).

[13] P. Jeszenszki, V. Rassolov, P. R. Surján, and A. Szabados, Mol. Phys. (2014), in press.

[14] P. R. Surjan, A. Szabados, P. Jeszenszki, and T. Zoboki, J. Math. Chem. **50**, 534 (2012).

[15] E. Rosta and P. R. Surjan, J. Chem. Phys. **116**, 878 (2002).

[16] V. A. Rassolov, J. Chem. Phys. **117**, 5978 (2002).

[17] V. A. Rassolov, F. Xu, and S. Garashchuk, J. Chem. Phys. **120**, 10385 (2004).

[18] S. Li, J. Ma, and Y. Jiang, J. Chem. Phys. **118**, 5736 (2003).

[19] J. Ma, S. H. Li, and W. Li, J. Comput. Chem. **27**, 39 (2006).

[20] M. Tarumi, M. Kobayashi, and H. Nakai, Int. J. Quantum Chem. **113**, 239 (2013).

[21] K. Pernal and J. Cioslowski, Ann. Phys. (Berlin) **13**, 194 (2004).

[22] K. Pernal, Comp. Theor. Chem. **1003**, 127 (2013).

[23] G. Gidofalvi and D. A. Mazziotti, J. Chem. Phys. **127**, 244105 (2007).

[24] G. Gidofalvi and D. A. Mazziotti, J. Chem. Phys. **129**, 134108 (2008).

[25] D. A. Mazziotti, Phys. Rev. A **76**, 052502 (2007).

[26] C. A. Schwerdtfeger and D. A. Mazziotti, J. Chem. Phys. **137**, 034107 (2012).

[27] E. Neuscamman, Phys. Rev. Lett. **109**, 203001 (2012).

[28] E. Neuscamman, J. Chem. Phys. **139**, 181101 (2013).

[29] G. K.-L. Chan and S. Sharma, Annu. Rev. Phys. Chem. **62**, 465 (2011).

[30] D. Ghosh, J. Hachmann, T. Yanai, and G. K.-L. Chan, J. Chem. Phys. **128**, 144117 (2008).

[31] Y. Kurashige and T. Yanai, J. Chem. Phys. **135**, 094104 (2011).

[32] F. Liu, Y. Kurashige, T. Yanai, and K. Morokuma, J. Chem. Theory Comput. **9**, 4462 (2013).

[33] J. Paldus, J. Čížek, and M. Takahashi, Phys. Rev. A **30**, 2193 (1984).

[34] J. Paldus, M. Takahashi, and R. W. H. Cho, Phys. Rev. B **30**, 4267 (1984).

[35] P. Piecuch and J. Paldus, Theor. Chem. Acc. **78**, 65 (1990), 10.1007/BF01119191.

[36] P. Piecuch, S. Zarrabian, J. Paldus, and J. Čížek, Phys. Rev. B **42**, 3351 (1990).

[37] J. Paldus and P. Piecuch, Int. J. Quantum Chem. **42**, 135 (1992).

[38] P. Piecuch, R. Tobola, and J. Paldus, Int. J. Quantum Chem. **55**, 133 (1995).

[39] P. Piecuch, A. E. Kondo, V. Spirko, and J. Paldus, J. Chem. Phys. **104**, 4699 (1996).

[40] D. W. Small and M. Head-Gordon, J. Chem. Phys. **137**, 114103 (2012).

[41] D. Kats and F. R. Manby, J. Chem. Phys. **139**, 021102 (2013).

[42] D. Kats, J. Chem. Phys. **141**, 061101 (2014).

[43] R. J. Bartlett and J. Noga, Chem. Phys. Lett. **150**, 29 (1988).

[44] T. Van Voorhis and M. Head-Gordon, Chem. Phys. Lett. **330**, 585 (2000).

[45] P.-D. Fan, K. Kowalski, and P. Piecuch, Mol. Phys. **103**, 2191 (2005).

[46] P.-D. Fan and P. Piecuch, Adv. Quantum Chem. **51**, 1 (2006).

[47] P. J. Knowles and B. Cooper, J. Chem. Phys. **133**, 224106 (2010).

[48] J. B. Robinson and P. J. Knowles, J. Chem. Phys. **135**, 044113 (2011).

[49] J. B. Robinson and P. J. Knowles, J. Chem. Phys. **136**, 054114 (2012).

[50] J. B. Robinson and P. J. Knowles, Phys. Chem. Chem. Phys. **14**, 6729 (2012).

[51] J. B. Robinson and P. J. Knowles, J. Chem. Phys. **138**, 074104 (2013).

[52] W. Meyer, Int. J. Quantum Chem. **S5**, 341 (1971).

[53] R. Ahlrichs, H. Lischka, V. Staemmler, and W. Kutzelnigg, J. Chem. Phys. **62**, 1225 (1975).

[54] K. Jankowski and J. Paldus, Int. J. Quantum Chem. **18**, 1243 (1980).

[55] F. Wennmohs and F. Neese, Chem. Phys. **343**, 217 (2008).

[56] J.-P. Malrieu, H. Zhang, and J. Ma, Chem. Phys. Lett. **493**, 179 (2010).

[57] B. G. Adams, K. Jankowski, and J. Paldus, Phys. Rev. A **24**, 2316 (1981).

[58] B. G. Adams, K. Jankowski, and J. Paldus, Phys. Rev. A **24**, 2330 (1981).

[59] R. A. Chiles and C. E. Dykstra, Chem. Phys. Lett. **80**, 69 (1981).

[60] S. M. Bachrach, R. A. Chiles, and C. E. Dykstra, J. Chem. Phys. **75**, 2270 (1981).

[61] R. J. Bartlett and M. Musial, The Journal of Chemical Physics **125**, 204105 (2006).

[62] L. M. J. Huntington and M. Nooijen, J. Chem. Phys. **133**, 184109 (2010).

[63] F. Neese, A. Hansen, F. Wennmohs, and S. Grimme, Acc. Chem. Res. **42**, 641 (2009), pMID: 19296607.

[64] L. M. J. Huntington, A. Hansen, F. Neese, and M. Nooijen, J. Chem. Phys. **136**, 064101 (2012).

[65] D. W. Small and M. Head-Gordon In preparation.

[66] F. E. Harris and H. A. Pohl, J. Chem. Phys. **42**, 3648 (1965).

[67] F. E. Harris, J. Chem. Phys. **43**, S17 (1965).

[68] E. G. Larson, Int. J. Quantum Chem. **2**, 83 (1968).

[69] R. Lefebvre and Y. G. Smeyers, Int. J. Quantum Chem. **1**, 403 (1967).

[70] O. Mårtensson and Y. Öhrn, Theor. Chim. Acta **9**, 133 (1967).

[71] E. Brändas, Int. J. Quantum Chem. **2**, 37 (1968).

[72] E. Brändas, J. Mol. Spectrosc. **27**, 236 (1968).

[73] E. Brändas and O. Mårtensson, Chem. Phys. Lett. **3**, 315 (1969).

[74] C. Coulson and R. J. White, Mol. Phys. **18**, 577 (1970).

[75] J. A. Pople, Int. J. Quantum Chem. **5**, 175 (1971).

[76] N. S. Ostlund, J. Chem. Phys. **57**, 2994 (1972).

[77] V. Bonačić-Koutecký and J. Koutecký, Theor. Chim. Acta **36**, 149 (1975).

[78] V. Bonačić-Koutecký and J. Koutecký, Theor. Chim. Acta **36**, 163 (1975).

[79] A. Toyota, T. Tanaka, and T. Nakajima, Int. J. Quantum Chem. **10**, 917 (1976).

[80] R. Seeger and J. A. Pople, J. Chem. Phys. **66**, 3045 (1977).

[81] K. Yamaguchi, Y. Yoshioka, T. Takatsuka, and T. Fueno, Theor. Chim. Acta **48**, 185 (1978).

[82] W. D. Edwards, Int. J. Quantum Chem. **34**, 549 (1988).

[83] H. Fukutome, Int. J. Quantum Chem. **20**, 955 (1981).

[84] J. Musher, Chem. Phys. Lett. **7**, 397 (1970).

[85] J. Hendeković, Chem. Phys. Lett. **21**, 205 (1973).

[86] J. Hendeković, Int. J. Quantum Chem. **8**, 799 (1974).

[87] J. Hendeković, Int. J. Quantum Chem. **10**, 1025 (1976).

[88] K. Hirao and H. Nakatsuji, J. Chem. Phys. **69**, 4535 (1978).

[89] L. Radom, P. C. Hariharan, J. A. Pople, and P. V. R. Schleyer, J. Am. Chem. Soc. **95**, 6531 (1973).

[90] H. Fukutome, Prog. Theor. Phys. **50**, 1433 (1973).

[91] R. C. Haddon, D. Poppinger, and L. Radom, J. Am. Chem. Soc. **97**, 1645 (1975).

[92] J. D. Dill, P. v. R. Schleyer, and J. A. Pople, J. Am. Chem. Soc. **97**, 3402 (1975).

[93] K. Krogh-Jespersen, J. Am. Chem. Soc. **107**, 537 (1985).

[94] G. J. Mains, C. W. Bock, and M. Trachtman, J. Phys. Chem. **94**, 5449 (1990).

[95] P. A. Limacher, T. D. Kim, P. W. Ayers, P. A. Johnson, S. De Baerdemacker, D. Van Neck, and P. Bultinck, Mol. Phys. **112**, 853 (2014).

[96] M. C. Böhm, Ber. Bunsenges. Phys. Chem. **85**, 755 (1981).

[97] M. C. Böhm, Chem. Phys. Lett. **83**, 533 (1981).

[98] M. C. Böhm, Int. J. Quantum Chem. **24**, 185 (1983).

[99] R. A. Horn and C. R. Johnson, *Matrix Analysis* (Cambridge University Press, New York, 2013), 2nd edition.

[100] F.B. Bobrowicz and W.A. Goddard, in *Methods of Electronic Structure Theory 3*, edited by H.F. Schaefer (Plenum, New York, 1977), p. 79.

[101] A. T. Amos and G. G. Hall, Proc. R. Soc. Lond. A **263**, 483 (1961).

[102] Y. Shao, L. Fusti-Molnar, Y. Jung, J. Kussmann, C. Ochsenfeld, S. T. Brown, A. T. B. Gilbert, L. V. Slipchenko, S. V. Levchenko, D. P. O'Neill, R.A. Distasio, Jr., R. C. Lochan, T. Wang, G. J. O. Beran, N. A. Besley, J. M. Herbert, C. Y. Lin, T. Van Voorhis, S. H. Chien, A. Sodt, R. P. Steele, V. A. Rassolov, P. E. Maslen, P. P. Korambath, R. D. Adamson, B. Austin, J. Baker, E. F. C. Byrd, H. Dachsel, R. J. Doerksen, A. Dreuw, B. D. Dunietz, A. D. Dutoi, T. R. Furlani, S. R. Gwaltney, A. Heyden, S. Hirata, C. P. Hsu, G. Kedziora, R. Z. Khalliulin, P. Klunzinger, A. M. Lee, M. S. Lee, W. Liang, I. Lotan, N. Nair, B. Peters, E. I. Proynov, P. A. Pieniazek, Y. M. Rhee, J. Ritchie, E. Rosta, C. D. Sherrill, A. C. Simmonett, J. E. Subotnik, H. L. Woodcock III, W. Zhang, A. T. Bell, A. K. Chakraborty, D. M. Chipman, F. J. Keil, A. Warshel, W. J. Hehre, H. F. Schaefer III, J. Kong, A. I. Krylov, P. M. W. Gill, and M. Head-Gordon, Phys. Chem. Chem. Phys. **8**, 3172 (2006).

[103] C. Sanderson, Armadillo: An open source c++ linear algebra library for fast prototyping and computationally intensive experiments, Technical report, NICTA, Australia (2010).

[104] P. Pulay, Chem. Phys. Lett. **73**, 393 (1980).

[105] P. Pulay, J. Comp. Chem. **3**, 556 (1982).

[106] J. Nocedal and S. J. Wright, *Numerical optimization* (Springer, New York, 2006), 2nd edition.

[107] T. Van Voorhis and M. Head-Gordon, Mol. Phys. **100**, 1713 (2002).

[108] E. R. Davidson, J. Comp. Phys. **17**, 87 (1975).

[109] T. H. Dunning, J. Chem. Phys. **90**, 1007 (1989).

[110] A. D. Becke, Phys. Rev. A **38**, 3098 (1988).

[111] C. Lee, W. Yang, and R. G. Parr, Phys. Rev. B **37**, 785 (1988).

[112] A. D. Becke, J. Chem. Phys. **98**, 5648 (1993).

[113] P. J. Stephens, F. J. Devlin, C. F. Chabalowski, and M. J. Frisch, J. Phys. Chem. **98**, 11623 (1994).

[114] G. D. Purvis and R. J. Bartlett, J. Chem. Phys. **76**, 1910 (1982).

[115] K. Raghavachari, G. W. Trucks, J. A. Pople, and M. Head-Gordon, Chem. Phys. Lett. **157**, 479 (1989).

[116] K. Hirao, Chem. Phys. Lett. **190**, 374 (1992).

[117] K. Hirao, Chem. Phys. Lett. **196**, 397 (1992).

[118] R. J. Buenker, S. D. Peyerimhoff, and W. Butscher, Mol. Phys. **35**, 771 (1978).

[119] B. O. Roos and P. E. M. Siegbahn, Int. J. Quantum Chem. **17**, 485 (1980).

[120] H.-J. Werner and P. J. Knowles, J. Chem. Phys. **89**, 5803 (1988).

[121] M. R. A. Blomberg and P. E. M. Siegbahn, J. Chem. Phys. **78**, 5682 (1983).

[122] B. O. Roos, Adv. Chem. Phys. **69**, 399 (1987).

[123] B. O. Roos, P. R. Taylor, and P. E. M. Siegbahn, Adv. Chem. Phys. **48**, 157 (1980).

[124] K. Ruedenberg, M. W. Schmidt, M. M. Gilbert, and S. T. Elbert, Chem. Phys. **71**, 41 (1982).

[125] K. Ruedenberg, M. W. Schmidt, and M. M. Gilbert, Chem. Phys. **71**, 51 (1982).

[126] K. Ruedenberg, M. W. Schmidt, M. M. Gilbert, and S. T. Elbert, Chem. Phys. **71**, 65 (1982).

[127] M. W. Schmidt and M. S. Gordon, Annu. Rev. Phys. Chem. **49**, 233 (1998).

[128] P. Siegbahn, A. Heiberg, B. Roos, and B. Levy, Physica Scripta **21**, 323 (1980).

[129] P. E. M. Siegbahn, J. Almlöf, A. Heiberg, and B. O. Roos, J. Chem. Phys. **74**, 2384 (1981).

[130] M. W. Schmidt, K. K. Baldridge, J. A. Boatz, S. T. Elbert, M. S. Gordon, J. H. Jensen, S. Koseki, N. Matsunaga, K. A. Nguyen, S. J. Su, T. L. Windus, M. Dupuis, and J. A. Montgomery, J. Comput. Chem. **14**, 1347 (1993).

[131] T. Williams, C. Kelley, and many others, Gnuplot 4.6: an interactive plotting program, `http://www.gnuplot.info` (2012).

[132] A. J. W. Thom and M. Head-Gordon, Phys. Rev. Lett. **101**, 193001 (2008).

[133] X. Li and J. Paldus, J. Chem. Phys. **128**, 144119 (2008).

[134] L. Bytautas, N. Matsunaga, and K. Ruedenberg, J. Chem. Phys. **132**, 074307 (2010).

[135] A. Halkier, T. Helgaker, P. Jørgensen, W. Klopper, and J. Olsen, Chem. Phys. Lett. **302**, 437 (1999).

[136] T. Helgaker, W. Klopper, H. Koch, and J. Noga, J. Chem. Phys. **106**, 9639 (1997).

[137] R. A. Kendall, T. H. Dunning, and R. J. Harrison, J. Chem. Phys. **96**, 6796 (1992).

[138] G. D. Purvis, R. Shepard, F. B. Brown, and R. J. Bartlett, Int. J. Quantum Chem. **23**, 835 (1983).

[139] U. S. Mahapatra, B. Datta, B. Bandyopadhyay, and D. Mukherjee, Adv. Quantum Chem. **30**, 163 (1998).

[140] U. S. Mahapatra, B. Datta, and D. Mukherjee, J. Chem. Phys. **110**, 6171 (1999).

[141] F. A. Evangelista, M. Hanauer, A. Köhn, and J. Gauss, J. Chem. Phys. **136**, 204108 (2012).

[142] D. I. Lyakh, M. Musial, V. F. Lotrich, and R. J. Bartlett, Chem. Rev. **112**, 182 (2012).

[143] C. A. Jiménez-Hoyos, R. Rodríguez-Guzmán, and G. E. Scuseria, J. Chem. Phys. **139**, 224110 (2013).

[144] J. Brabec, H. J. J. van Dam, J. Pittner, and K. Kowalski, J. Chem. Phys. **136**, 124102 (2012).

[145] Z. Chen and M. R. Hoffmann, J. Chem. Phys. **137**, 014108 (2012).

[146] J. P. Coe, D. J. Taylor, and M. J. Paterson, J. Chem. Phys. **137**, 194111 (2012).

[147] O. Demel, S. Kedzuch, M. Svana, S. Ten-no, J. Pittner, and J. Noga, Phys. Chem. Chem. Phys. **14**, 4753 (2012).

[148] P. R. Nagy and A. Szabados, Int. J. Quantum Chem. **113**, 230 (2013).

[149] R. Shepard, G. Gidofalvi, and S. R. Brozell, J. Chem. Phys. **141**, 064105 (2014).

[150] N. X. Wang and A. K. Wilson, J. Chem. Phys. **121**, 7632 (2004).

[151] T. V. Russo, R. L. Martin, and P. J. Hay, J. Chem. Phys. **102**, 8023 (1995).

[152] M. Filatov and D. Cremer, Phys. Chem. Chem. Phys. **5**, 2320 (2003).

[153] B. Santra, A. Michaelides, and M. Scheffler, J. Chem. Phys. **131**, 124509 (2009).

[154] C. W. Bauschlicher, Jr. and H. Partridge, Chem. Phys. Lett. **231**, 277 (1994).

[155] K. E. Edgecombe and A. D. Becke, Chem. Phys. Lett. **244**, 427 (1995).

[156] J. G. Smith, *Organic Chemistry*, chapter Supplementary Topic C (McGraw-Hill, New York, 2011), 3rd edition, url: http://highered.mheducation.com/sites/dl/free/0073375624/825564/Pericyclic_Reactions.pdf (accessed Aug 24, 2014).

[157] R. B. Woodward and R. Hoffmann, J. Am. Chem. Soc. **87**, 395 (1965).

[158] J. I. Brauman and D. M. Golden, J. Am. Chem. Soc. **90**, 1920 (1968).

[159] G. B. Gill, Q. Rev. Chem. Soc. **22**, 338 (1968).

[160] M. J. S. Dewar and C. A. Ramsden, J. Chem. Soc., Perkin Trans. 1 pp. 1839–1844 (1974).

[161] N. J. Turro and A. Devaquet, J. Am. Chem. Soc. **97**, 3859 (1975).

[162] R. Huisgen, Angew. Chem. Int. Ed. Engl. **16**, 572 (1977).

[163] P. S. Lee, S. Sakai, P. Hörstermann, W. R. Roth, E. A. Kallel, and K. N. Houk, J. Am. Chem. Soc. **125**, 5839 (2003).

[164] X. L. Fan, Y. F. Zhang, W. M. Lau, and Z. F. Liu, Phys. Rev. B **72**, 165305 (2005).

[165] C. R. Hickenboth, J. S. Moore, S. R. White, N. R. Sottos, J. Baudry, and S. R. Wilson, Nature **446**, 423 (2007).

[166] M. T. Ong, J. Leiding, H. Tao, A. M. Virshup, and T. J. Martínez, J. Am. Chem. Soc. **131**, 6377 (2009).

[167] J. Breulet and H. F. Schaefer, J. Am. Chem. Soc. **106**, 1221 (1984).

[168] J. M. Oliva, J. Gerratt, P. B. Karadakov, and D. L. Cooper, J. Chem. Phys. **107**, 8917 (1997).

[169] S. Sakai, J. Phys. Chem. A **110**, 6339 (2006).

[170] M. Olivucci, I. N. Ragazos, F. Bernardi, and M. A. Robb, J. Am. Chem. Soc. **115**, 3710 (1993).

[171] P. Celani, F. Bernardi, M. Olivucci, and M. A. Robb, J. Chem. Phys. **102**, 5733 (1995).

[172] F. Sicilia, L. Blancafort, M. J. Bearpark, and M. A. Robb, J. Phys. Chem. A **111**, 2182 (2007).

[173] S. Sakai, Chem. Phys. Lett. **287**, 263 (1998).

[174] S. Sakai, Chem. Phys. Lett. **319**, 687 (2000).

[175] B. Dick, Y. Haas, and S. Zilberg, Chem. Phys. **347**, 65 (2008).

[176] Y. Harabuchi, S. Maeda, T. Taketsugu, N. Minezawa, and K. Morokuma, J. Chem. Theory Comput. **9**, 4116 (2013).

[177] I. Özkan, A. Kinal, and M. Balci, J. Phys. Chem. A **108**, 507 (2004).

[178] C. Silva López, O. Nieto Faza, and A. R. de Lera, Chem. Eur. J. **13**, 5009 (2007).

[179] K. Ishida, K. Morokuma, and A. Komornicki, J. Chem. Phys. **66**, 2153 (1977).

[180] B. C. Garrett, M. J. Redmon, R. Steckler, D. G. Truhlar, K. K. Baldridge, D. Bartol, M. W. Schmidt, and M. S. Gordon, J. Phys. Chem. **92**, 1476 (1988).

[181] C. Gonzalez and H. B. Schlegel, J. Phys. Chem. **94**, 5523 (1990).

[182] M. W. Schmidt, M. S. Gordon, and M. Dupuis, J. Am. Chem. Soc. **107**, 2585 (1985).

[183] K. A. Kistler and S. Matsika, J. Phys. Chem. A **111**, 2650 (2007).

[184] K. A. Kistler and S. Matsika, J. Chem. Phys. **128**, 215102 (2008).

[185] V. B. Delchev, Monatsh. Chem. **142**, 251 (2011).

[186] S. Yamazaki, A. L. Sobolewski, and W. Domcke, Phys. Chem. Chem. Phys. **11**, 10165 (2009).

[187] S. Yamazaki, W. Domcke, and A. L. Sobolewski, J. Phys. Chem. A **112**, 11965 (2008).

[188] S. Yamazaki and T. Taketsugu, J. Phys. Chem. A **116**, 491 (2012).

[189] L. Blancafort, D. González, M. Olivucci, and M. A. Robb, J. Am. Chem. Soc. **124**, 6398 (2002).

[190] H. J. Wörner and F. Merkt, J. Chem. Phys. **127**, 034303 (2007).

[191] W. Zou, M. Filatov, and D. Cremer, Int. J. Quantum Chem. **112**, 3277 (2012).

[192] W. T. Borden and E. R. Davidson, J. Am. Chem. Soc. **101**, 3771 (1979).

[193] S. Zilberg and Y. Haas, J. Am. Chem. Soc. **124**, 10683 (2002).

[194] E. P. F. Lee and T. G. Wright, Phys. Chem. Chem. Phys. **1**, 219 (1999).

[195] J. Feng, J. Leszczynski, B. Weiner, and M. C. Zerner, J. Am. Chem. Soc. **111**, 4648 (1989).

[196] W. J. Hehre and P. v. R. Schleyer, J. Am. Chem. Soc. **95**, 5837 (1973).

[197] M. N. Glukhovtsev, B. Reindl, and P. v. R. Schleyer, Mendeleev Commun. **3**, 100 (1993).

[198] R. C. Lochan and M. Head-Gordon, J. Chem. Phys. **126**, 164101 (2007).

[199] F. Neese, T. Schwabe, S. Kossmann, B. Schirmer, and S. Grimme, J. Chem. Theory Comput. **5**, 3060 (2009).

[200] U. Bozkaya, J. Chem. Theory Comput. **10**, 2371 (2014).

[201] See Supplementary Material Document No. (blank) for TS coordinates for the WHV reaction and extra PES plots for the polyatomic examples. For information on Supplementary Material, see http://www.aip.org/pubservs/epaps.html.

LIST OF FIGURES

FIGURES

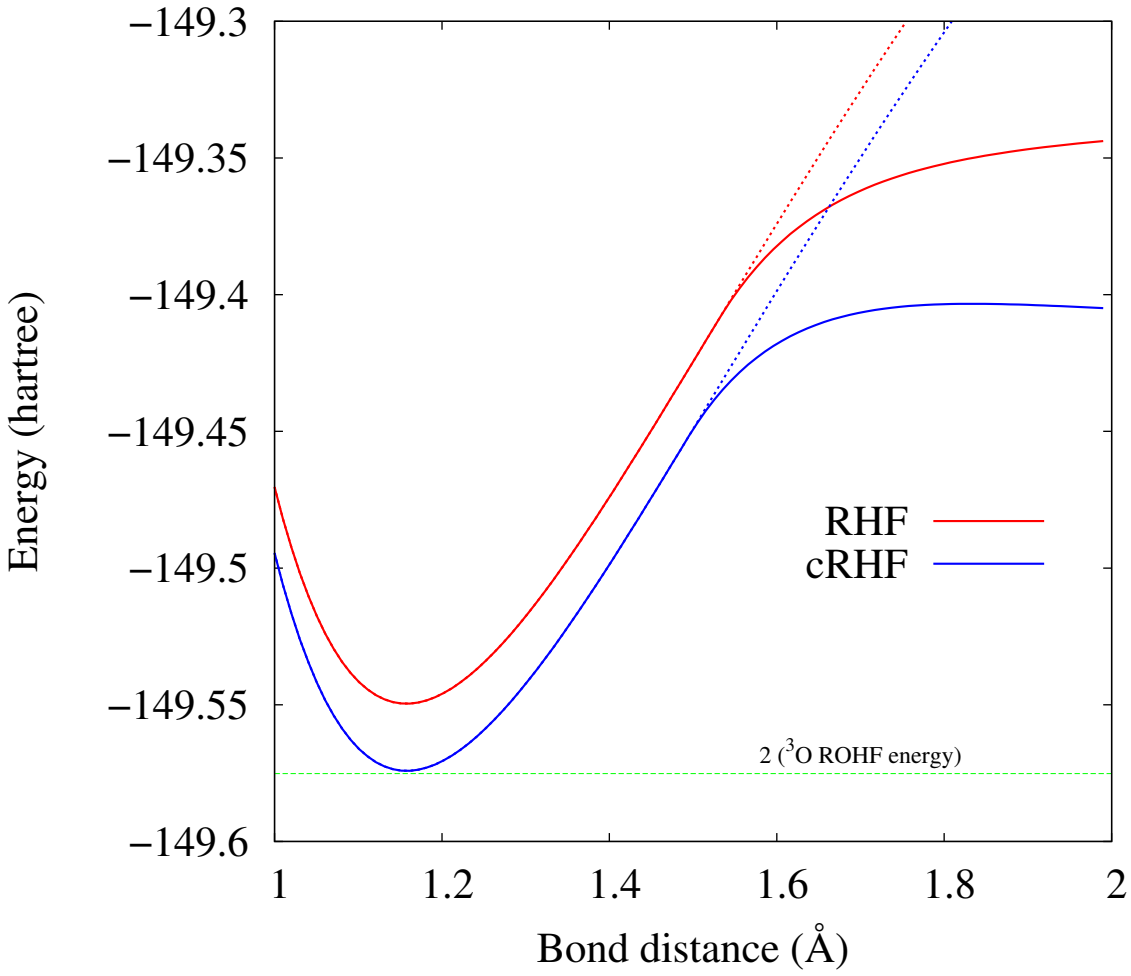

FIG. 1

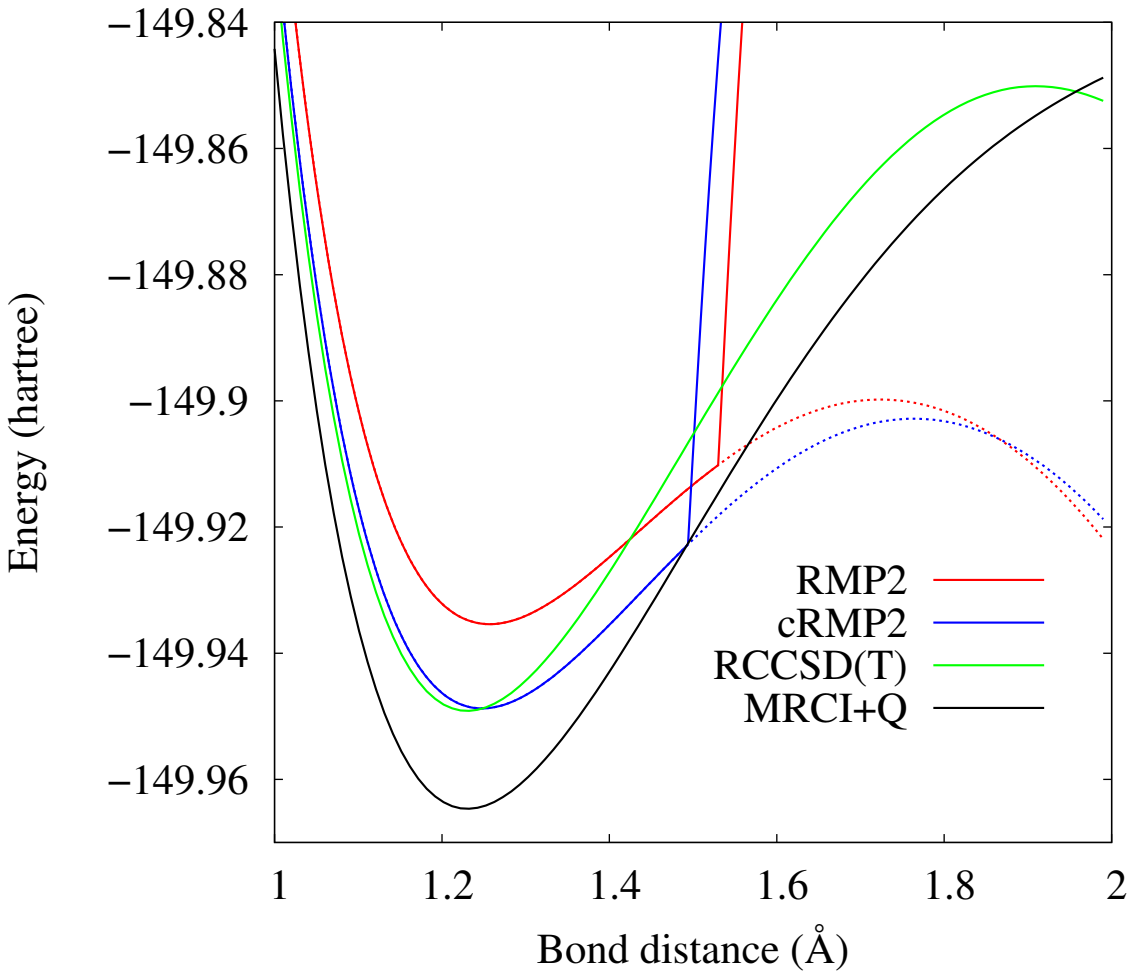
−149.84
−149.86
−149.88
−149.9
−149.92
−149.94
−149.96
Energy (hartree)
1
1.2
1.4
1.6
1.8
2
Bond distance (Å)
RMP2
cRMP2
RCCSD(T)
MRCI+Q

FIG. 2

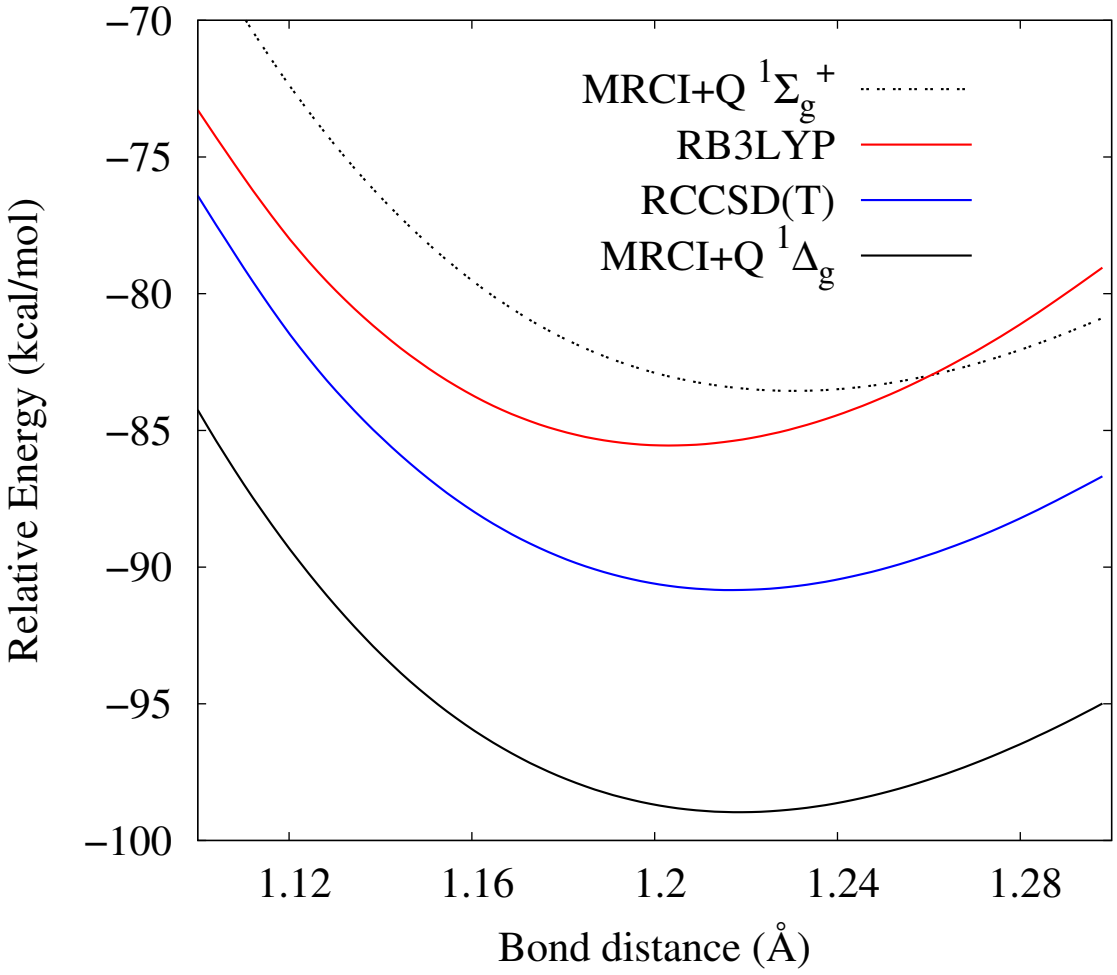
−70
−75
−80
−85
−90
−95
−100
Relative Energy (kcal/mol)
1.12
1.16
1.2
1.24
1.28
Bond distance (Å)
MRCI+Q $^1\Sigma_g^+$
RB3LYP
RCCSD(T)
MRCI+Q $^1\Delta_g$

FIG. 3

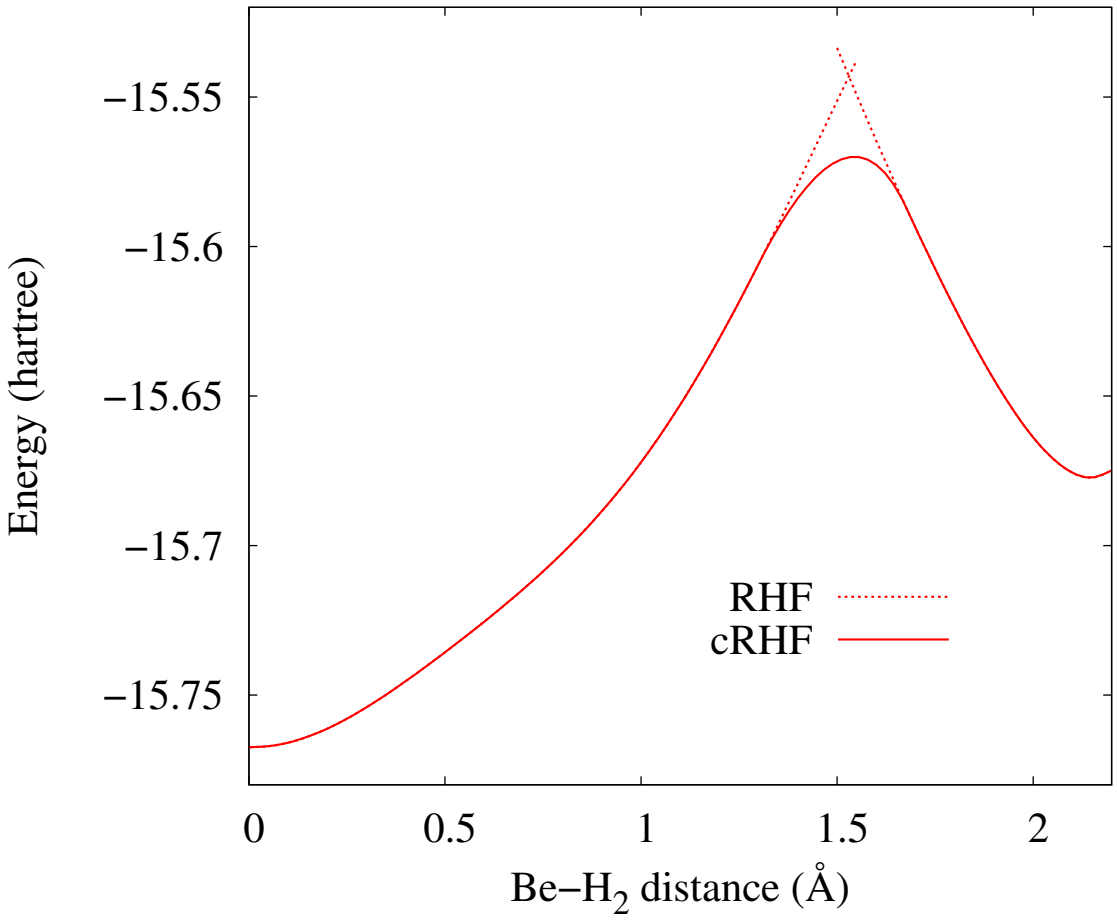
−15.55
−15.6
−15.65
−15.7
−15.75
Energy (hartree)
0
0.5
1
1.5
2
Be–H2 distance (Å)
RHF
cRHF

FIG. 4

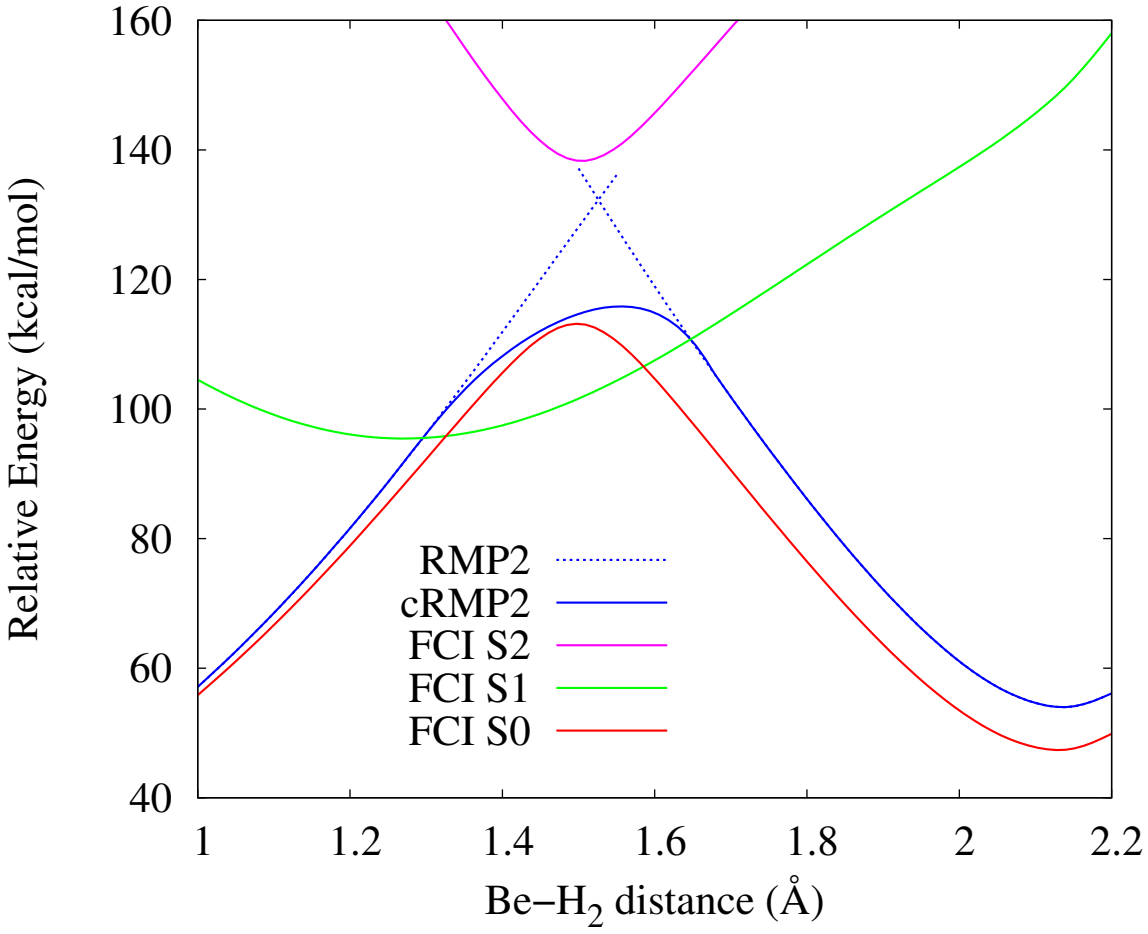
160
140
120
100
80
60
40
Relative Energy (kcal/mol)
1
1.2
1.4
1.6
1.8
2
2.2
Be–H2 distance (Å)
RMP2
cRMP2
FCI S2
FCI S1
FCI S0

FIG. 5

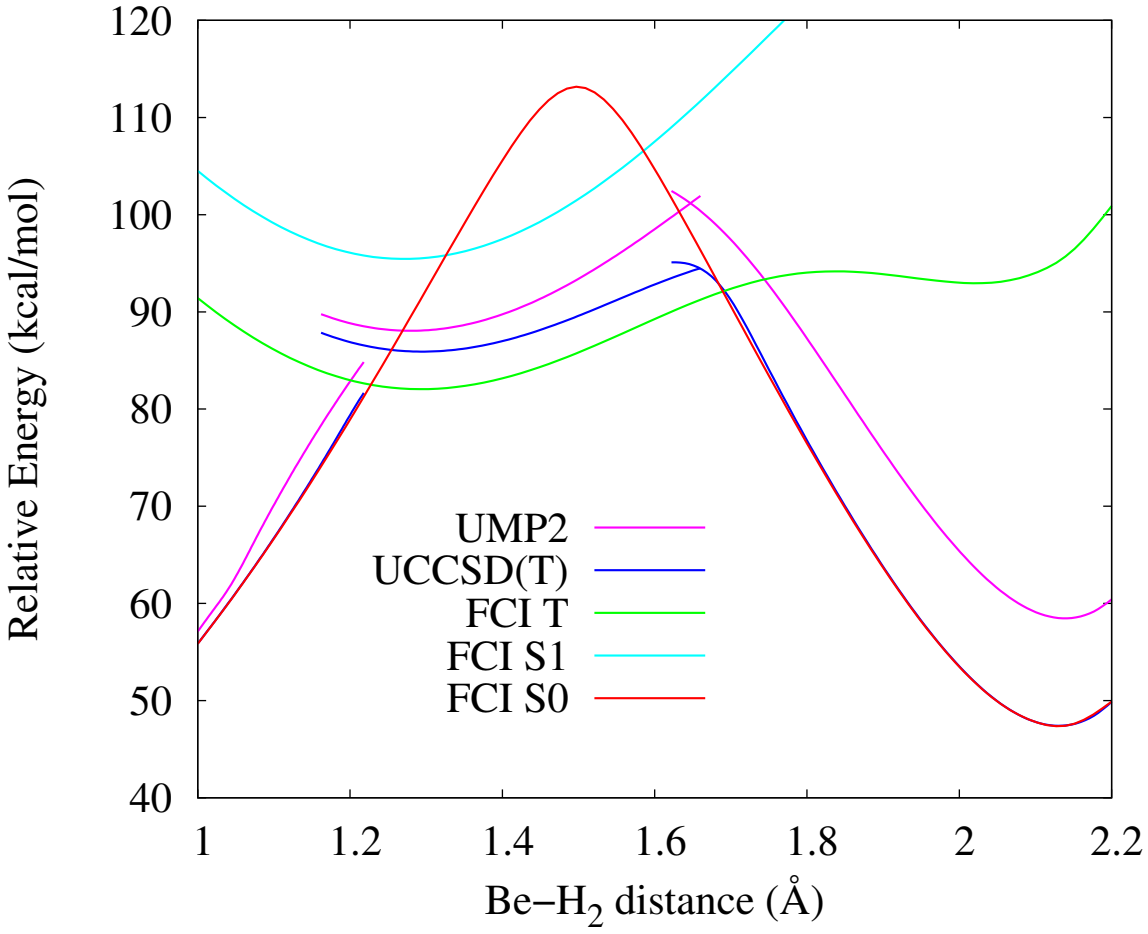
120
110
100
90
80
70
60
50
40
1
1.2
1.4
1.6
1.8
2
2.2
Relative Energy (kcal/mol)
Be–H2 distance (Å)
UMP2
UCCSD(T)
FCI T
FCI S1
FCI S0

FIG. 6

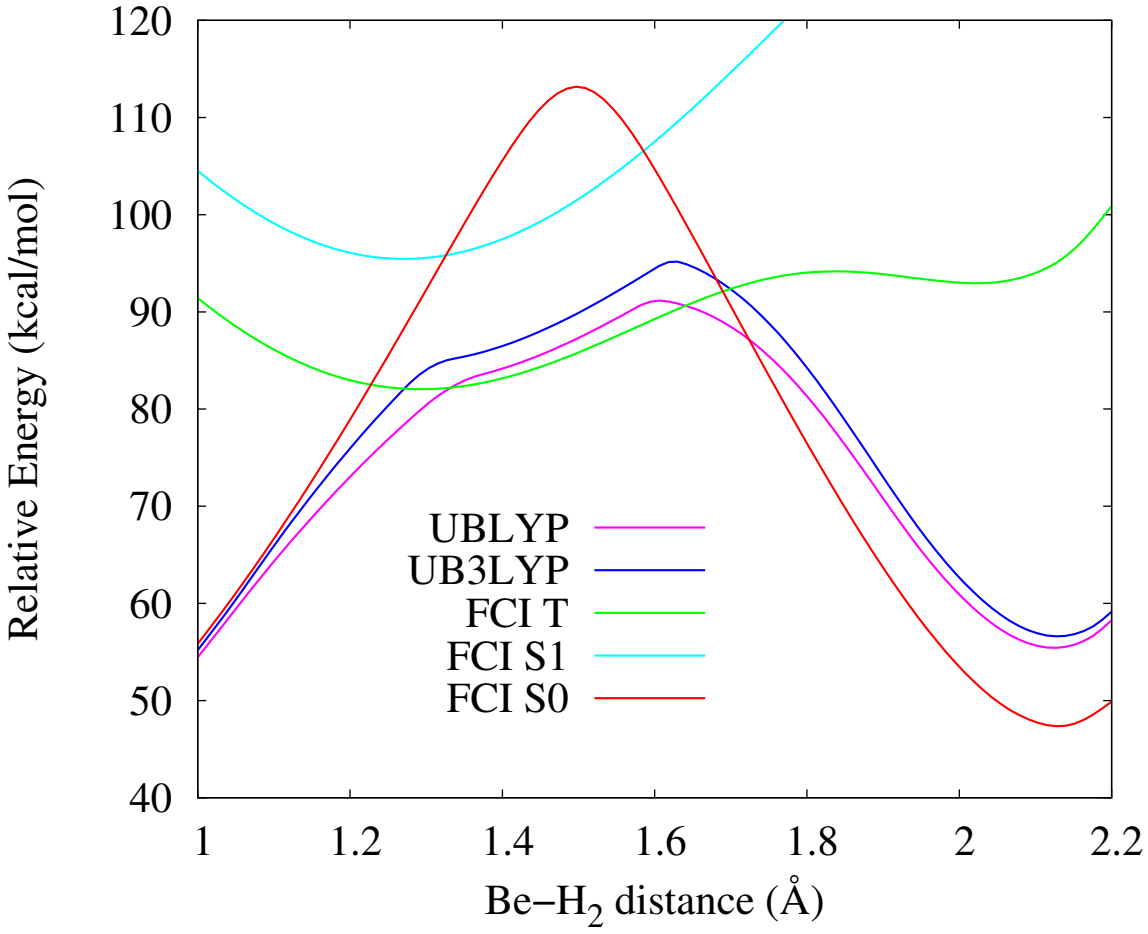
Relative Energy (kcal/mol)
120
110
100
90
80
70
60
50
40
1
1.2
1.4
1.6
1.8
2
2.2
Be–H2 distance (Å)
UBLYP
UB3LYP
FCI T
FCI S1
FCI S0

FIG. 7

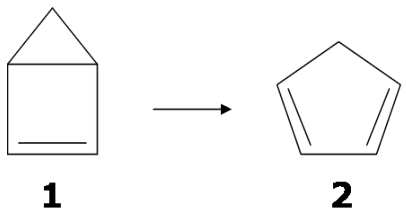
1
2

FIG. 8

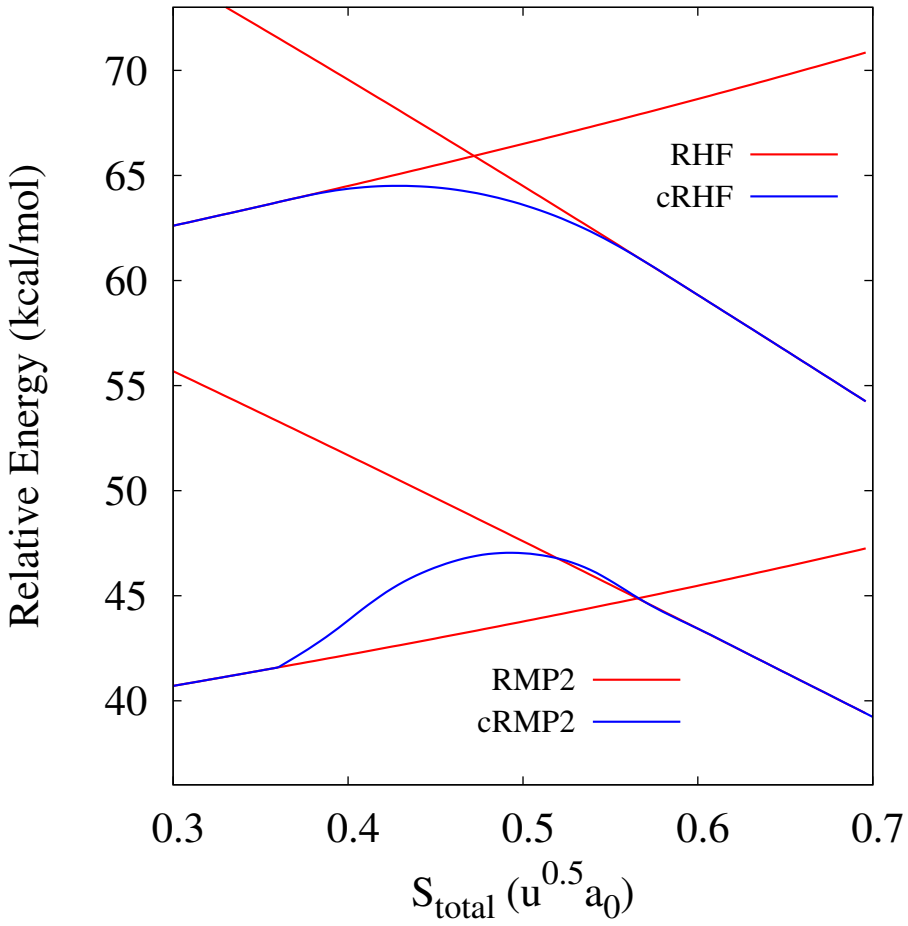
Relative Energy (kcal/mol)
70
65
60
55
50
45
40
0.3
0.4
0.5
0.6
0.7
S_total (u^0.5 a_0)
RHF
cRHF
RMP2
cRMP2

FIG. 9

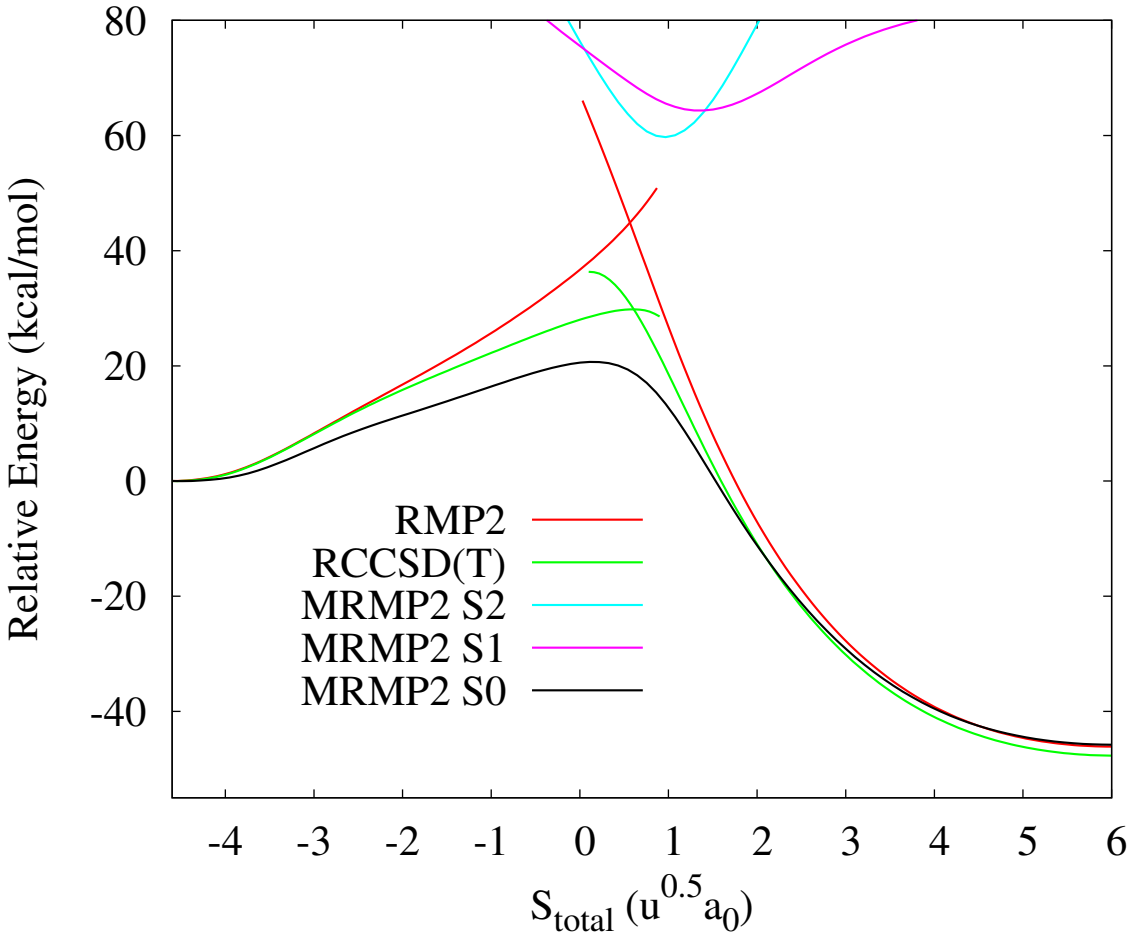
80
60
40
20
0
-20
-40
Relative Energy (kcal/mol)
-4
-3
-2
-1
0
1
2
3
4
5
6
S_total (u^0.5 a_0)
RMP2
RCCSD(T)
MRMP2 S2
MRMP2 S1
MRMP2 S0

FIG. 10

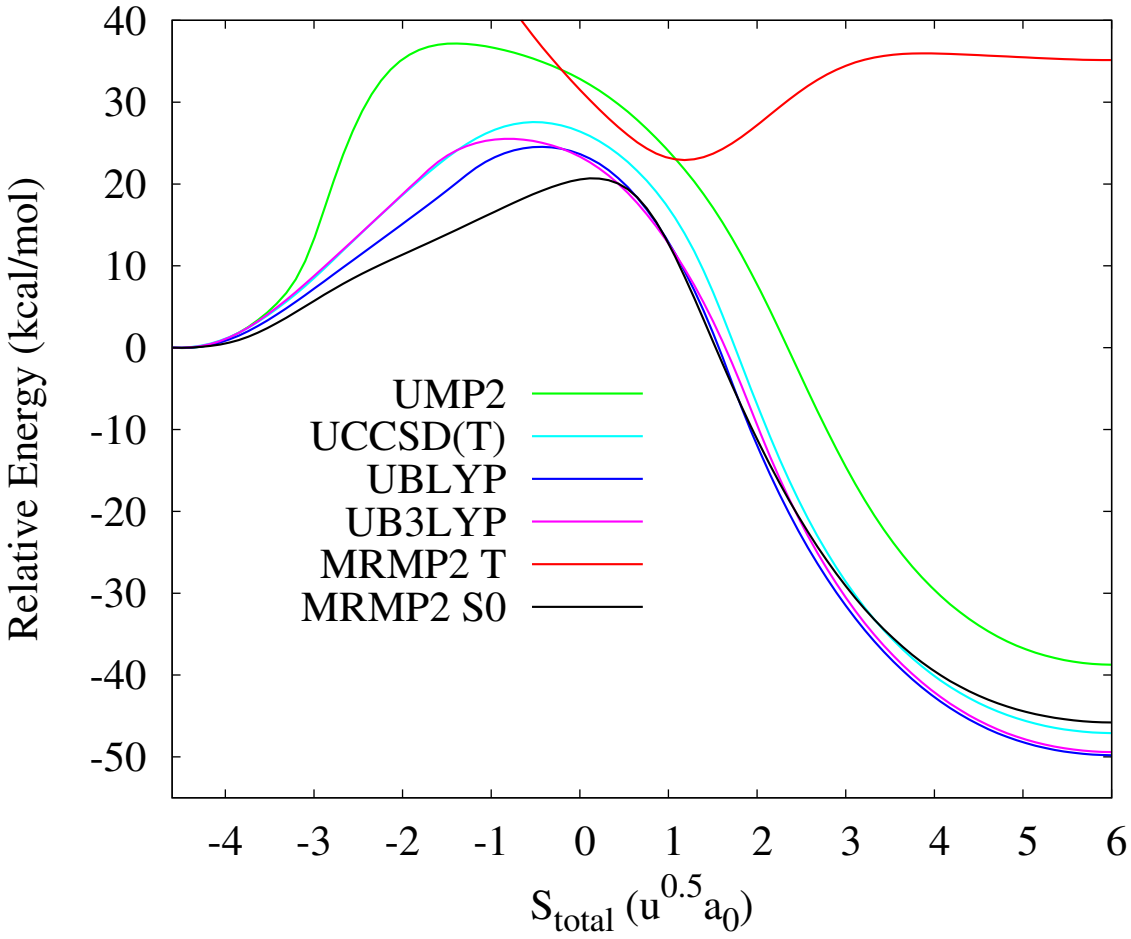
Relative Energy (kcal/mol)
40
30
20
10
0
-10
-20
-30
-40
-50
-4
-3
-2
-1
0
1
2
3
4
5
6
S_total (u^0.5 a_0)
UMP2
UCCSD(T)
UBLYP
UB3LYP
MRMP2 T
MRMP2 S0

FIG. 11

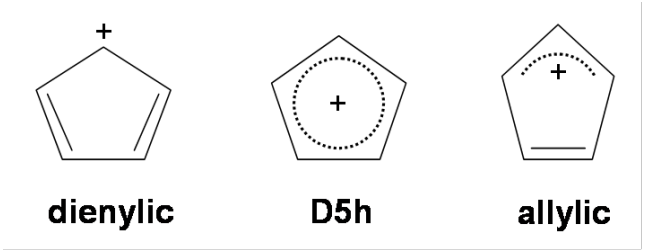
+
dienylic
+
D5h
+
allylic

FIG. 12

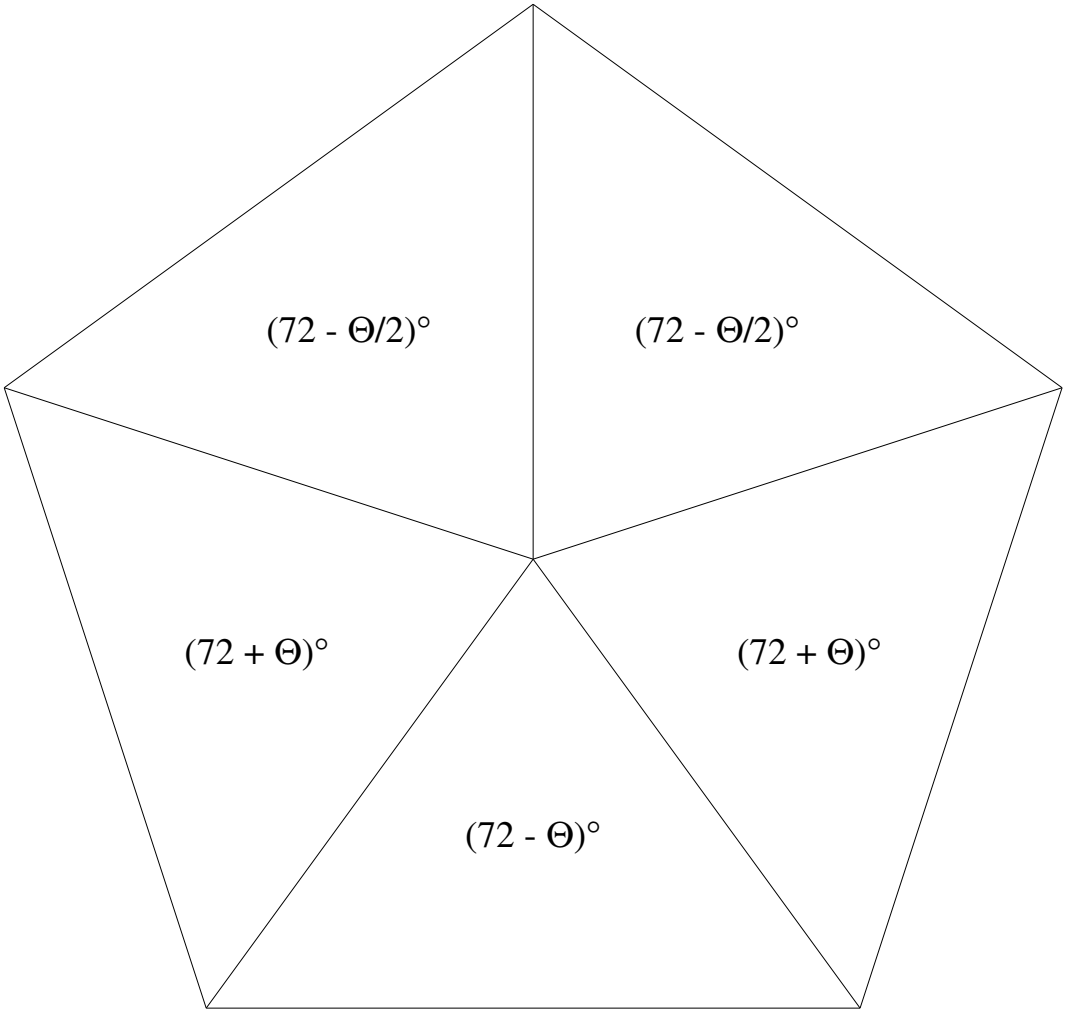

FIG. 13

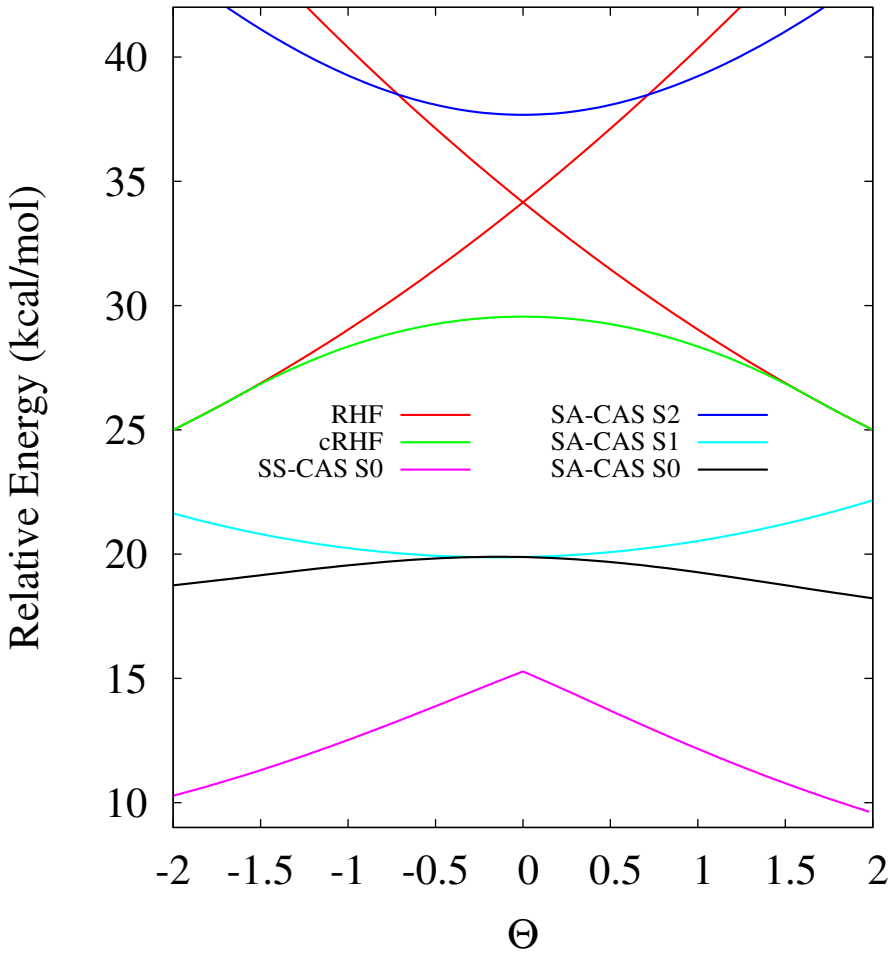
Relative Energy (kcal/mol)
40
35
30
25
20
15
10
-2
-1.5
-1
-0.5
0
0.5
1
1.5
2
Θ
RHF
cRHF
SS-CAS S0
SA-CAS S2
SA-CAS S1
SA-CAS S0

FIG. 14

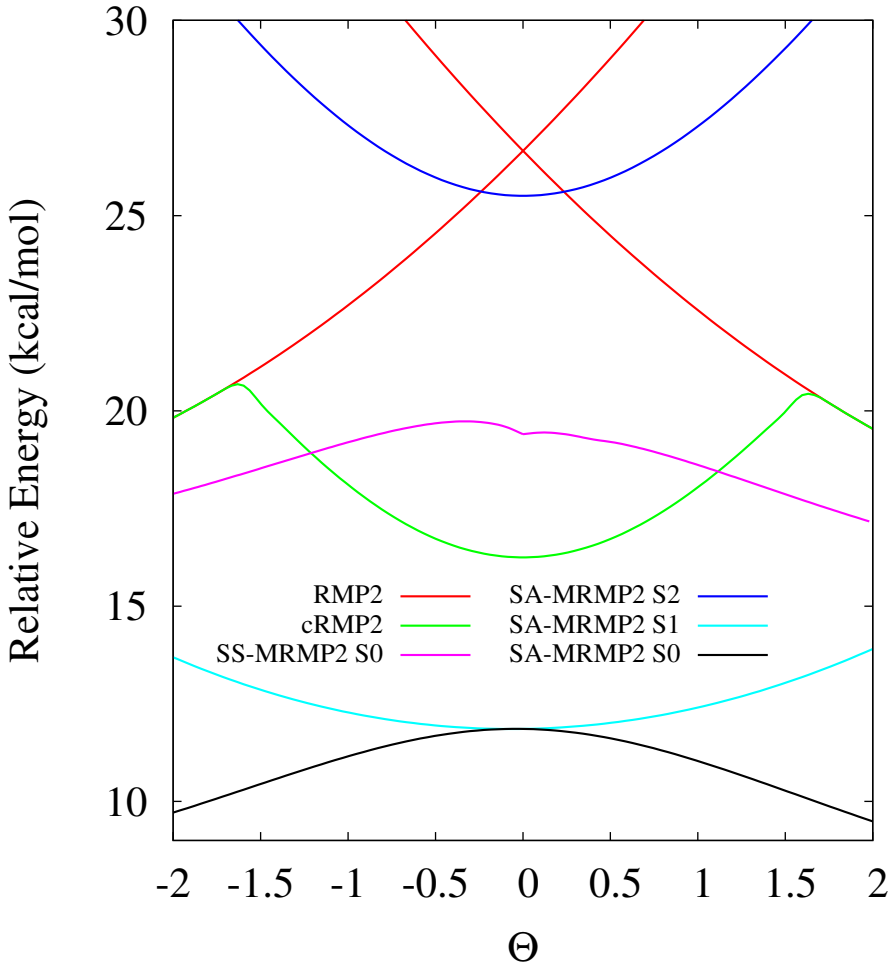
Relative Energy (kcal/mol)
30
25
20
15
10
-2
-1.5
-1
-0.5
0
0.5
1
1.5
2
Θ
RMP2
cRMP2
SS-MRMP2 S0
SA-MRMP2 S2
SA-MRMP2 S1
SA-MRMP2 S0

FIG. 15

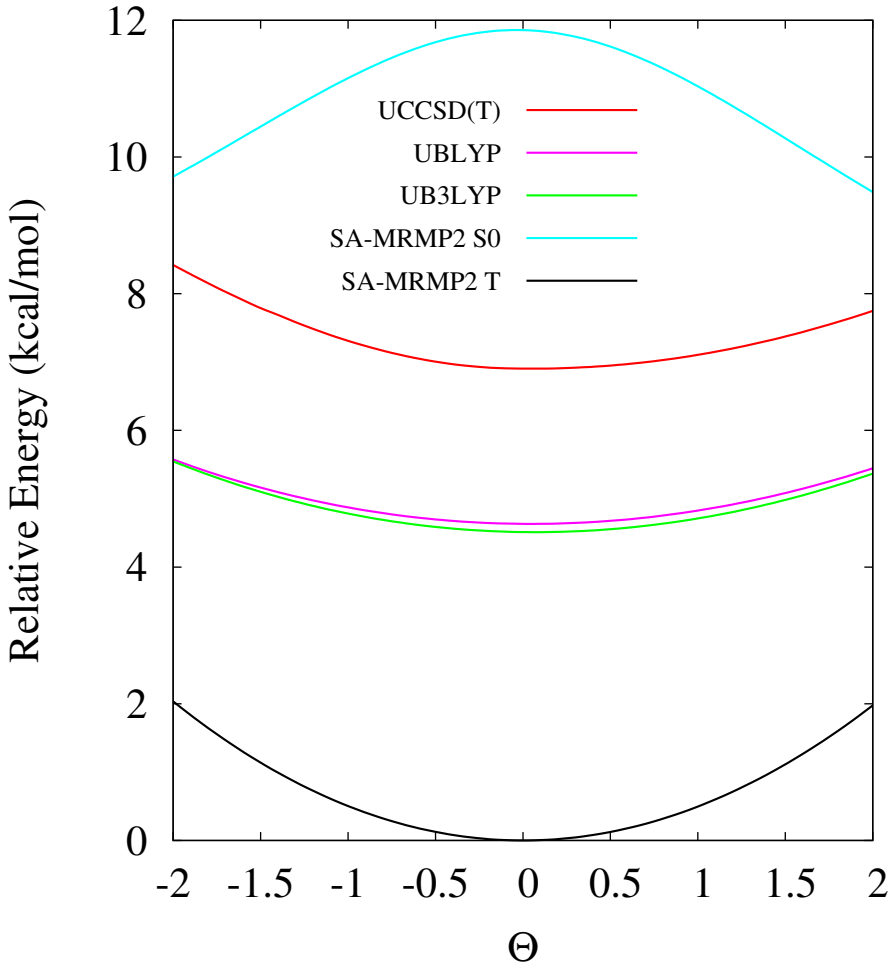
Relative Energy (kcal/mol)
12
10
8
6
4
2
0
-2
-1.5
-1
-0.5
0
0.5
1
1.5
2
Θ
UCCSD(T)
UBLYP
UB3LYP
SA-MRMP2 S0
SA-MRMP2 T

FIG. 16